5-1-2011

Global X-Ray Properties Of The O And B Stars In Carina

Y. Nazé

P. S. Broos

L. M. Oskinova

L. K. Townsley

David H. Cohen
Swarthmore College, dcohen1@swarthmore.edu

See next page for additional authors

The Astrophysical Journal Supplement Series, 194:7 (20pp), 2011 May doi:10.1088/0067-0049/194/1/7

GLOBAL X-RAY PROPERTIES OF THE O AND B STARS IN CARINA

Y. Nazé[1,14], P. S. Broos[2], L. Oskinova[3], L. K. Townsley[2],
and
D. Cohen[4], M. F. Corcoran[5,6], N. R. Evans[7], M. Gagné[8], A. F. J. Moffat[9,10], J. M. Pittard[11],
G. Rauw[1], A. ud-Doula[12], and N. R. Walborn[13]
[1] GAPHE, Département AGO, Université de Liège, Allée du 6 Août 17, Bat. B5C, B4000 Liège, Belgium; naze@astro.ulg.ac.be
[2] Department of Astronomy & Astrophysics, 525 Davey Laboratory, Pennsylvania State University, University Park, PA 16802, USA
[3] Institute for Physics and Astronomy, Universität Potsdam, 14476 Potsdam, Germany
[4] Swarthmore College Department of Physics and Astronomy, 500 College Avenue, Swarthmore, PA 19081, USA
[5] CRESST and X-ray Astrophysics Laboratory, NASA/GSFC, Greenbelt, MD 20771, USA
[6] Universities Space Research Association, 10211 Wincopin Circle, Suite 500 Columbia, MD 21044, USA
[7] Harvard-Smithsonian Center for Astrophysics, 60 Garden Street, Cambridge, MA 02138, USA
[8] Department of Geology and Astronomy, West Chester University, West Chester, PA 19383, USA
[9] Département de Physique, Université de Montréal, Succursale Centre-Ville, Montréal, QC, H3C 3J7, Canada
[10] Centre de recherche en astrophysique du Québec, Canada
[11] School of Physics and Astronomy, The University of Leeds, Leeds LS2 9JT, UK
[12] Penn State Worthington Scranton, 120 Ridge View Drive, Dunmore, PA 18512, USA
[13] Space Telescope Science Institute, 3700 Martin Drive, Baltimore, MD 21218, USA
Received 2010 November 10; accepted 2011 February 4; published 2011 April 28

ABSTRACT

The key empirical property of the X-ray emission from O stars is a strong correlation between the bolometric and X-ray luminosities. In the framework of the *Chandra* Carina Complex Project, 129 O and B stars have been detected as X-ray sources; 78 of those, all with spectral type earlier than B3, have enough counts for at least a rough X-ray spectral characterization. This leads to an estimate of the L_X–L_{BOL} ratio for an exceptional number of 60 O stars belonging to the same region and triples the number of Carina massive stars studied spectroscopically in X-rays. The derived $\log(L_X/L_{BOL})$ is −7.26 for single objects, with a dispersion of only 0.21 dex. Using the properties of hot massive stars listed in the literature, we compare the X-ray luminosities of different types of objects. In the case of O stars, the L_X–L_{BOL} ratios are similar for bright and faint objects, as well as for stars of different luminosity classes or spectral types. Binaries appear only slightly harder and slightly more luminous in X-rays than single objects; the differences are not formally significant (at the 1% level), except for the L_X–L_{BOL} ratio in the medium (1.0–2.5 keV) energy band. Weak-wind objects have similar X-ray luminosities but they display slightly softer spectra compared with "normal" O stars with the same bolometric luminosity. Discarding three overluminous objects, we find a very shallow trend of harder emission in brighter objects. The properties of the few B stars bright enough to yield some spectral information appear to be different overall (constant X-ray luminosities, harder spectra), hinting that another mechanism for producing X-rays, besides wind shocks, might be at work. However, it must be stressed that the earliest and X-ray brightest among these few detected objects are similar to the latest O stars, suggesting a possibly smooth transition between the two processes.

Key words: ISM: individual objects (Carina nebula) – stars: massive – X-rays: stars

Online-only material: color figures

1. INTRODUCTION

The existence of X-ray emission from hot, massive stars was predicted three decades ago by Cassinelli & Olson (1979) and it was serendipitously discovered at the same time during early observations by the *Einstein* satellite; massive O stars in the Carina Nebula were among the first detections (Seward et al. 1979). It was immediately found that the X-ray emission of these O stars was proportional to their optical luminosity (Harnden et al. 1979). The relation was then refined to be proportional to their bolometric luminosity (Pallavicini et al. 1981; as the first observations dealt with stars of similar types and reddening, both relations were equivalent). X-rays are now thought to be generated in wind shocks and, as the winds are line-driven, it may seem quite natural that a relationship between X-ray and bolometric luminosities exists. However, the theoretical derivation of this relationship is not obvious: Owocki & Cohen (1999) showed that, while the X-ray luminosity "naturally" scales with the wind density parameter $\dot{M}/v_\infty$, it only scales with the bolometric luminosity if there is "a delicate balance between X-ray emission and absorption" and "a special form for the radial distribution of wind shocks." A better knowledge of this relationship may thus yield a better understanding of the X-ray emission of O stars. Finally, *Einstein* observations also showed that the detection rate of B stars was much lower than that of O stars (Grillo et al. 1992).

The X-ray properties of O and B stars were constrained more accurately by Berghöfer et al. (1997) using the *ROSAT* All-Sky Survey (RASS). Using 237 detections, Berghöfer et al. confirmed the decline in the detection rate toward later spectral types (all stars with type O7 or earlier were detected as X-ray sources, while at most 10% of B3–B9 stars were detected). This fact, correlated with a higher incidence of variability and binarity among the latest types, led to the conclusion that low-mass pre-main-sequence (PMS) companions could be responsible for the X-ray emission of late-B stars. Berghöfer et al. also confirmed that the $\log(L_X/L_{BOL}) \sim -7$ relation applies down

[14] Research Associate FRS-FNRS

to $\log(L_{BOL}) \sim 38$ erg s^{-1} (corresponding approximately to spectral type B1III–V) although with a large dispersion (σ of 0.4 dex, or a factor of 2.5). Cohen et al. (1997) further showed a steep decrease in X-ray luminosity (with $\log(L_X/L_{BOL})$ reaching −8.5 at B2) and a softening of the emission for fainter stars. At the same time, studies of O+OB binaries revealed enhanced X-ray luminosities for these objects, attributed to the collision between the two stellar winds (Chlebowski 1989). No such enhancement was reported for B+B binaries (even early-B binaries) but such systems were much less studied than O+OB binaries.

In recent years, many star clusters were observed by *XMM-Newton* or *Chandra*, often for detailed studies of the PMS population or the diffuse emission (e.g., Güdel et al. 2007; Townsley et al. 2003). Only a few of these clusters harbor a significantly large number of O stars, which is required for statistical studies of their X-ray properties. The O star data also often had limited signal-to-noise, preventing a full spectral analysis of the X-ray emission. In the favorable cases, estimates of the X-ray luminosities appeared compatible with the $\log(L_X/L_{BOL}) \sim -7$ relation, although a large scatter was often present due to limited knowledge of the stellar content (Nazé et al. 2008; Wang et al. 2008). Some rare, peculiar objects were overluminous in X-rays, as exemplified by the Orion Trapezium (Stelzer et al. 2005). Only in a few cases could in-depth studies of the L_X–L_{BOL} relation be performed. These analyses relied on a precise knowledge of the cluster's stellar content and detailed stellar properties (multiplicity, reddening, bolometric luminosity, and X-ray spectrum). They revealed a rather tight L_X–L_{BOL} relation (e.g., NGC 6231, Sana et al. 2006; Car OB1, Antokhin et al. 2008). Only a few O+OB binaries were found to be truly overluminous (see also Oskinova 2005); X-ray-bright wind–wind collisions thus now appear to be the exception rather than the rule, although a detailed physical explanation is still lacking.

However, the RASS and cluster samples differed in many ways (see Nazé 2011, for a full discussion), notably regarding the number of targets analyzed (>200 versus ∼20), their homogeneity (a mix of different clusters and field stars for the former versus a single cluster/association for the latter) and the data quality (count rates and hardness ratios versus detailed spectral analyses). The first attempt to combine both approaches was recently performed by Nazé (2009). This global spectral analysis of the massive stars detected in the 2XMM catalog confirmed the lack of overluminosities in binaries as well as the large scatter around the L_X–L_{BOL} relation for an inhomogeneous population, hinting at differences between clusters.

This very large *Chandra* program targeting the Carina Complex now constitutes a new opportunity to look at the X-ray properties of a large population of massive stars, with better homogeneity between stars than in the 2XMM sample. This paper aims at more than tripling the number of massive stars analyzed in Carina in the X-ray domain compared to what is available at the present time (Antokhin et al. 2008). Section 2 will summarize the data characteristics, Section 3 presents the derived L_X–L_{BOL} relation, and Sections 4– 7 discuss the hardness of the spectra, the properties of binaries, the weak-wind stars, and the faintest objects, respectively. Finally, Section 8 summarizes our results.

2. THE DATA

The *Chandra* Carina Complex Project (CCCP) is described in detail in Townsley et al. (2011). The source detection process and spectral extractions are described by Broos et al. (2010, 2011). Broos et al. also describe the complicated completeness limits of the survey, which vary across the field due to *Chandra*'s changing point-spread function, vignetting, and the spatially complex exposure times across the mosaic.

Parallel to the X-ray data analysis, a list of 70 O-type and 130 B-type stars in the CCCP field of view was compiled from Skiff (2009; see also Gagné et al. 2011), a catalog of stars that have been studied spectroscopically in the literature. We concentrate on these OB stars in this paper because their spectral types are known. A discussion of candidate O and B stars, derived from photometric data, is given in Povich et al. (2011) and Evans et al. (2011). Note that all but 3 of the 130 B-type stars have spectral types earlier than B3; they can thus be considered as hot, massive objects. The three later-type B stars are undetected in X-rays; these three sources are not discussed thoroughly in this paper.

For a distance of 2.3 kpc, the bolometric luminosities of the catalog objects were generally derived from the known spectral types and spectral energy distribution fitting (Povich et al. 2011) using *UBVJHK*s magnitudes and *Spitzer*-IRAC photometry. This ensures that the derived values of the bolometric luminosities do not depend greatly on the choice of the extinction law; other systematic errors (due, e.g., to the choice of atmospheric models) are <5% (Povich et al. 2011). In only 17 cases, bolometric luminosities were derived from *V*-magnitudes and bolometric corrections due to the lack of reliable photometry (Povich et al. 2011; Gagné et al. 2011). Comparisons between the results of the two methods revealed only limited differences (<0.2 dex) between the bolometric luminosities. Povich et al. also derived reddenings from the photometry, leading to estimates of the interstellar absorbing column N_H(ISM). To this aim, we use a gas-to-dust ratio $N_H/A_V = 1.6 \times 10^{21}$ cm^2 mag^{-1} (Vuong et al. 2003; Getman et al. 2005) and $R_V = 4$. Such a value of R_V is adapted to the choice of a 2.3 kpc distance (Walborn 1995); it also provides the best fit for the photometry of O and B stars (Povich et al. 2011). Photometric uncertainties and star-to-star variations in extinction yield errors <20% in bolometric luminosities (Povich et al. 2011), but we acknowledge that a large scatter exists around the total-to-selective absorption, the used value being only the best currently available. The binary status of 15 O-type stars was obtained from Rauw et al. (2009, spectroscopic binaries) and Nelan et al. (2004, mostly visual binaries). Note that we used the same spectral type for QZ Car as Parkin et al. (2011). Four additional B stars are cataloged as binaries, because they appear as such in Nelan et al. (2004) or are listed as B+B in the Skiff (2009) catalog used for collecting spectral types.

This massive star catalog was first cross-correlated with the CCCP list of X-ray sources (Broos et al. 2011) and then used to directly explore the X-ray data at the positions of the hot stars (Gagné et al. 2011). In total, 129 matches were found (Table 1), or about 65% of the objects in the Skiff-based catalog of OB stars (see above). Carina's three Wolf-Rayet stars and the luminous blue variable η Carinae were also detected in the CCCP; they are mentioned in Townsley et al. (2011). Two O stars, 66 early-B stars, and the three late-B stars mentioned above remain undetected in the CCCP. This is consistent with the average completeness limit of this survey, $\log L_X \sim 30$ (Broos et al. 2011). Indeed, with a typical $\log(L_X/L_{BOL})$ of −7 and minimum bolometric luminosities of $\log L_{BOL} \sim 38.2$, all O-type stars are expected to be detected with such a limit and even to display

Table 1
Distribution of the Detected Hot Stars as a Function of the Recorded Counts

X-ray brightness	O, Single	O, Binaries	B, Single	B, Binaries
>100 counts	29	13	10	0
50–100 counts	16	2	8	0
<50 counts	8	0	41	2
Undetected	2	0	67	2

enough counts for at least a rough spectral analysis. On the contrary, most B stars have much lower bolometric luminosities and $\log(L_X/L_{BOL})$ ratios. The low detection rate in their case is therefore unsurprising; only the earliest-type and brightest objects could thus be analyzed here (see Evans et al. 2011 for more details on the faintest, undetected B stars).

2.1. Spectral Fitting

X-ray spectra were automatically extracted for all X-ray sources. Whenever several observations of the same target were available, the individual spectra were merged (but note that the far off-axis observations of QZ Car reported by Parkin et al. 2011 were not included in this study). Spectral fitting was done on the grouped spectra (grouped such that each spectral bin displays at least a signal-to-noise ratio of 3) of the 78 O and B sources which displayed at least 50 net counts. We arbitrarily split the sources in two groups: reliable if the source has at least 100 counts (which is the case for 29 single O stars, 13 O+OB binaries, and 10 B stars, see Table 1), and somewhat reliable if the source has 50–100 counts (true for 16 single O stars, 2 O+OB binaries, and 8 B stars). Errors are indeed larger for objects of the second group (see Table 2). The fitted models were of the form $tbabs_1 \times tbabs_2 \times \sum_1^{1or2} apec$. The *tbabs* components represent neutral absorptions (Wilms et al. 2000); the first one is fixed to the intervening interstellar column and the second one accounts for potential additional, circumstellar absorption. The small number of counts and the limited sensitivity at low energies prevented us from using more sophisticated wind absorption models. The last part of the model corresponds to the emission from one or two optically thin thermal plasmas (Smith et al. 2001). The second thermal plasma component was added only if necessary, i.e., if it led to a significant improvement in the χ^2 of the fit. The abundances were always kept to solar because the sources generally have too few counts to ascertain abundance determinations.

Table 2 provides the fitting results. Column 1 shows the X-ray source name, while Columns 2–4 give the observed basic source properties: the number of net counts in the 0.5–8.0 keV band together with their associated 68% confidence intervals, the photon flux (net counts divided by the mean effective area and the exposure time), and the median energy of the recorded counts (Broos et al. 2011). The next columns provide the fitting results themselves: the reduced χ^2, the number of degrees of freedom, the absorbing columns (interstellar then circumstellar), the temperatures and emission measures of each thermal component, and finally the observed fluxes in the 0.5–10.0 keV energy band (these energy boundaries were chosen to ease comparison with other, previous L_X–L_{BOL} studies). For each fitted parameter, the lower and upper limits of the 90% confidence intervals are listed as indices and exponents, respectively (if the limit is not explicitly noted, the parameter should be considered as unconstrained in that direction). Note that for the fluxes, these errors (estimated using the Xspec command *flux err*) are only indicative as they do not fully or correctly take into account the spectral model uncertainties and/or the correlations between spectral parameters.

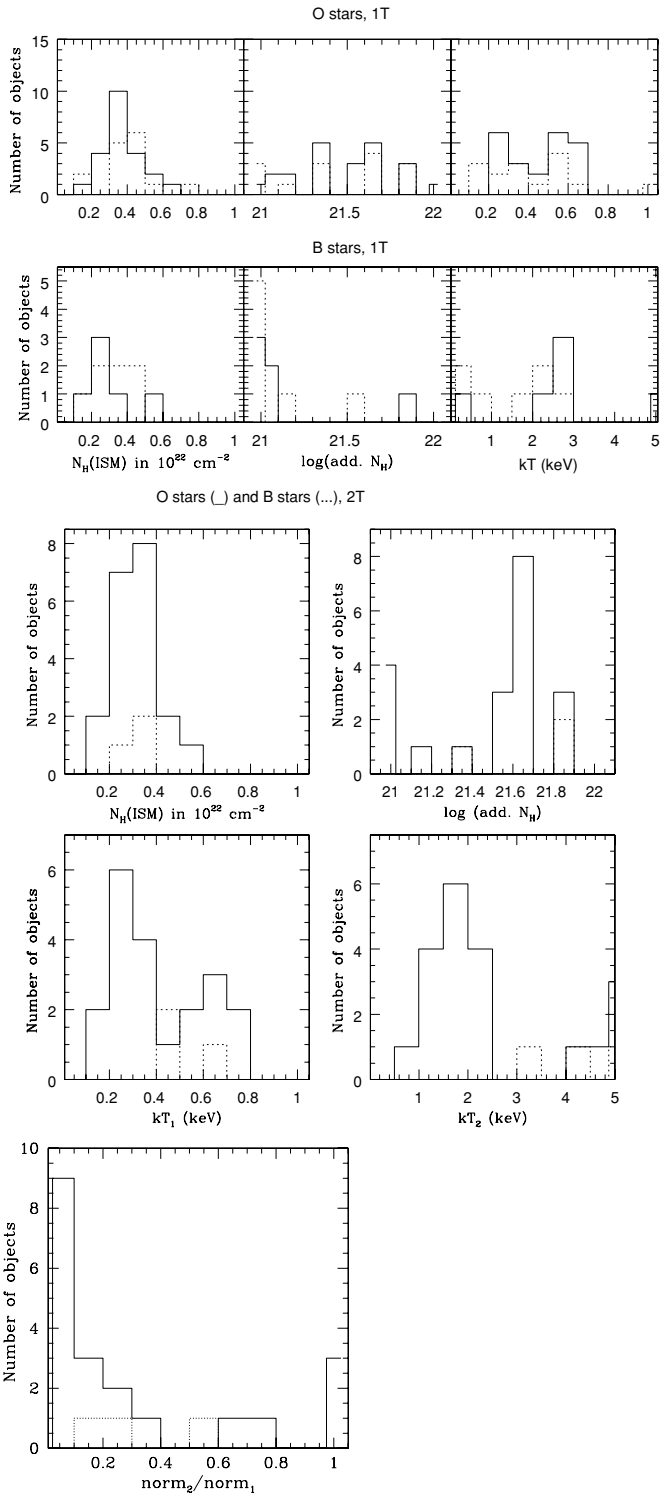

Figure 1. Distribution of the spectral parameters for O and B stars. For the top six subfigures, the solid line refers to sources with >100 counts and the dotted line to sources with 50–100 counts. For the bottom five subfigures, only the sources with >100 counts were considered, with O stars shown using a solid line and B stars as a dotted line.

Histograms of the temperatures and absorbing columns were derived from the best-fit values (Figure 1). The results are similar to those of Nazé (2009): for O-type stars, the favored kT is about 0.2–0.6 keV, a second temperature of about 2 keV is sometimes

Table 2
Best-fits Results for the Hot Stars Associated with X-ray Sources with >50 counts

CXOGNC J	Net Counts (counts)	Photon Flux (photons cm^{-2} s^{-1})	Med. En. (keV)	χ^2_ν	dof	$N_{\rm H}$(ISM) (10^{22} cm^{-2})	log($N_{\rm H}$)	kT_1 (keV)	log EM$_1$	kT_2 (keV)	log EM$_2$	Total Obs. Flux (10^{-14} erg cm^{-2} s^{-1})
104012.42−594810.1	416.8^{437}_{396}	3.39e-5	1.00	0.92	18	0.22	21.8 $^{+0.1}_{...}$	0.18 $^{+0.13}_{-0.03}$	56.2 $^{+0.3}_{-9.4}$	1.1 $^{+0.6}_{...}$	54.2 $^{+0.5}_{-0.3}$	$5.09^{5.2}_{1.87}$
104031.71−594643.9	131.1^{143}_{120}	9.55e-6	0.96	0.29	5	0.12	21.8 $^{+0.2}_{-0.4}$	0.24 $^{+0.15}_{-0.07}$	55.2 $^{+0.9}_{...}$	...	...	$1.53^{1.6}_{0.}$
104210.35−595800.9	$64.2^{72.7}_{56.3}$	5.40e-6	1.03	0.38	5	0.48	20.9 $^{+0.7}_{...}$	0.56 $^{+0.2}_{-0.3}$	54.0 $^{+0.7}_{-0.2}$	...	...	$0.74^{0.85}_{0.18}$
104243.71−595416.6	$106.6^{118}_{95.2}$	6.40e-6	0.91	0.87	3	0.14	21.6 $^{+0.2}_{...}$	0.20 $^{+0.1}_{...}$	55.0 $^{+0.4}_{-8.2}$	10.	53.3 $^{+0.4}_{-0.4}$	$1.64^{1.45}_{0.18}$
104311.17−594420.8	133.4^{145}_{122}	1.68e-5	0.97	0.39	5	0.37	21.5 $^{+0.3}_{...}$	0.30 $^{+0.3}_{-0.1}$	55.0 $^{+0.9}_{...}$	...	...	$2.03^{2.19}_{0.}$
104315.33−601204.3	$57.7^{65.4}_{50.1}$	1.45e-5	0.90	1.09	5	0.13	21.8 $^{+0.2}_{-0.3}$	0.14 $^{+0.07}_{-0.03}$	56.2	...	...	$1.6^{1.54}_{0.}$
104317.92−600803.1	122.7^{136}_{110}	5.68e-6	0.91	0.96	5	0.17	21.4 $^{+0.4}_{...}$	0.27 $^{+0.1}_{-0.1}$	54.5 $^{+1.3}_{-0.6}$	...	...	$1.11^{1.2}_{0.}$
104341.24−593548.1	$65.4^{73.7}_{57.2}$	6.10e-6	1.15	0.56	5	0.49	21.8 $^{+0.3}_{-0.5}$	0.44 $^{+0.2}_{-0.2}$	54.5 $^{+1.0}_{-0.5}$	...	...	$0.74^{0.89}_{0.}$
104343.42−602027.7	$59.6^{67.9}_{51.5}$	5.21e-6	0.90	0.80	5	0.25	20.8 $^{+1.1}_{...}$	0.28 $^{+0.1}_{-0.1}$	54.3 $^{+1.9}_{-0.4}$	...	...	$0.99^{1.00}_{0.}$
104343.55−593403.4	114.5^{125}_{104}	8.63e-6	1.54	1.32	5	0.50	16.9 $^{+4.5}_{...}$	2.7 $^{+1.3}_{-0.8}$	54.2 $^{+0.09}_{-0.08}$	...	...	$1.99^{2.36}_{1.24}$
104343.99−594817.9	$92.5^{106}_{78.7}$	5.11e-6	1.09	1.81	3	0.40	20.9 $^{+0.8}_{...}$	0.22 $^{+0.1}_{...}$	54.4 $^{+0.5}_{-0.7}$	1.7	53.5 $^{+0.2}_{-0.6}$	$0.86^{1.04}_{0.12}$
104345.04−595325.0	$93.1^{104}_{82.4}$	7.70e-6	1.32	0.86	5	0.20	17.8 $^{+4.4}_{...}$	2.0 $^{+0.9}_{-1.3}$	54.0 $^{+0.79}_{-0.09}$	...	...	$1.4^{1.61}_{0.98}$
104346.69−593254.7	$73.0^{81.9}_{64}$	1.45e-5	0.99	0.20	3	0.38	16.7 $^{+5.2}_{...}$	0.21 $^{+0.1}_{...}$	54.7 $^{+0.5}_{-7.9}$	1.1 $^{+1.7}_{...}$	53.9 $^{+0.5}_{-0.3}$	$2.28^{2.18}_{0.22}$
104348.70−593324.2	$86.6^{96}_{77.2}$	6.54e-6	1.04	0.50	5	0.41	21.3 $^{+0.5}_{...}$	0.53 $^{+0.2}_{-0.3}$	54.2 $^{+0.8}_{-0.3}$	...	...	$0.90^{0.98}_{0.}$
104353.63−593328.4	$74.5^{83.2}_{65.8}$	7.62e-6	1.20	1.52	5	0.43	21.8 $^{+0.2}_{...}$	0.67 $^{+0.8}_{-0.3}$	54.3 $^{+0.4}_{-0.4}$	...	...	$0.84^{0.94}_{0.23}$
104354.40−593257.4	519.5^{543}_{497}	1.18e-4	1.00	1.53	24	0.35	21.4 $^{+0.2}_{-0.5}$	0.39 $^{+0.12}_{-0.09}$	55.4 $^{+0.3}_{-0.3}$	...	...	$9.12^{9.56}_{2.74}$
104355.36−593248.8	$89.0^{98.6}_{79.6}$	1.17e-5	0.99	0.91	5	0.39	21.7 $^{+0.2}_{...}$	0.19 $^{+0.28}_{-0.06}$	55.6 $^{+1.1}_{-8.8}$	...	...	$1.32^{1.35}_{0.}$
104357.47−593251.3	$2976.8^{3.03E+03}_{2.92E+03}$	3.43e-4	1.39	0.58	62	0.37	21.9 $^{+0.05}_{-0.06}$	0.54 $^{+0.03}_{-0.04}$	56.3 $^{+0.09}_{-0.09}$	1.7 $^{...}_{-0.2}$	55.4 $^{+0.1}_{-0.3}$	$66.2^{69.6}_{58.6}$
104357.46−600528.3	$90.9^{101}_{81.1}$	8.40e-6	0.91	0.87	5	0.19	20.9 $^{+0.8}_{...}$	0.30 $^{+0.1}_{-0.2}$	54.4 $^{+1.7}_{-0.3}$	...	...	$1.5^{1.59}_{0.}$
104357.65−593253.7	685.9^{713}_{659}	5.08e-5	0.97	0.89	31	0.35	15.5 $^{+5.3}_{...}$	0.51 $^{+0.06}_{-0.05}$	54.9 $^{+0.2}_{-0.2}$	...	...	$7.38^{7.33}_{1.76}$
104357.96−593353.4	$102.5^{113}_{92.4}$	7.71e-6	1.41	1.08	5	0.37	17.6 $^{+4.6}_{...}$	2.1 $^{+0.8}_{-1.6}$	54.1 $^{+0.61}_{-0.08}$	...	...	$1.52^{1.77}_{1.13}$
104358.45−593301.5	$82.9^{92.2}_{73.8}$	6.15e-6	1.28	0.49	3	0.39	22.2 $^{+0.2}_{-0.3}$	0.14 $^{+0.5}_{...}$	56.7 $^{+0.6}_{...}$	4.9	53.8 $^{...}_{-0.3}$	$1.42^{1.48}_{0.}$
104359.92−593225.4	$98.3^{108}_{88.4}$	1.45e-5	0.90	2.04	5	0.32	21.4 $^{+0.3}_{...}$	0.23 $^{+0.14}_{-0.07}$	55.0 $^{+0.8}_{-0.7}$	...	...	$1.61^{1.66}_{0.}$
104400.17−600607.7	$87.8^{97.9}_{77.8}$	7.56e-6	1.45	0.59	5	0.17	21.1 $^{+0.9}_{...}$	2.5 $^{+2.2}_{-1.3}$	54.0 $^{+0.2}_{-0.1}$	...	...	$1.64^{1.94}_{1.19}$
104400.16−600509.8	358.6^{378}_{340}	3.02e-5	0.97	0.72	17	0.23	21.7 $^{+0.1}_{-0.4}$	0.24 $^{+0.13}_{-0.05}$	55.6 $^{+0.5}_{-0.9}$	...	...	$4.85^{4.98}_{0.}$
104400.38−595227.5	288.5^{307}_{270}	2.39e-5	1.03	1.24	12	0.35	21.0 $^{+0.4}_{...}$	0.63 $^{+0.08}_{-0.09}$	54.6 $^{+0.2}_{-0.1}$	...	...	$3.48^{3.72}_{2.15}$
104405.09−593341.4	$58.6^{66.4}_{51}$	4.36e-6	1.48	0.78	5	0.43	16.5 $^{+5.7}_{...}$	2.5 $^{+1.3}_{-1.9}$	53.8 $^{+0.8}_{-0.1}$	...	...	$0.94^{1.16}_{0.54}$
104405.84−593511.6	162.7^{176}_{150}	8.47e-6	1.35	1.37	4	0.36	21.9 $^{+0.1}_{-0.4}$	0.68 $^{+0.1}_{-0.1}$	54.4 $^{+0.3}_{-0.5}$	9.8	53.6 $^{+0.4}_{-0.3}$	$1.73^{1.71}_{0.46}$
104407.26−593430.5	303.3^{317}_{283}	5.46e-5	1.06	0.58	9	0.32	21.6 $^{+0.2}_{...}$	0.20 $^{+0.10}_{-0.05}$	56.0 $^{+0.4}_{-1.0}$	1.4 $^{+1.0}_{-0.3}$	54.6 $^{+0.1}_{-0.2}$	$8.59^{9.24}_{2.44}$
104408.84−593434.4	522.3^{546}_{499}	3.97e-5	1.01	0.74	22	0.31	20.9 $^{+0.6}_{...}$	0.33 $^{+0.15}_{-0.07}$	55.0 $^{+0.3}_{-0.2}$	1.6 $^{+1.1}_{-0.4}$	54.2 $^{+0.1}_{-0.2}$	$6.49^{6.86}_{2.35}$
104409.08−593435.3	424.7^{446}_{404}	3.23e-5	1.03	0.81	20	0.34	21.4 $^{+0.2}_{-0.3}$	0.54 $^{+0.05}_{-0.09}$	54.9 $^{+0.2}_{-0.1}$	...	...	$4.52^{4.78}_{3.52}$
104411.04−600321.8	119.9^{131}_{109}	1.27e-5	1.10	0.71	4	0.22	21.6 $^{+0.3}_{...}$	0.44 $^{+0.3}_{-0.2}$	54.4 $^{+0.5}_{-0.7}$	4.6	53.6 $^{+0.4}_{-6.8}$	$2.04^{2.28}_{0.48}$
104413.19−594310.1	359.2^{305}_{294}	5.36e-5	1.42	0.73	17	0.64	22.1 $^{+0.07}_{-0.07}$	0.62 $^{+0.14}_{-0.08}$	55.5 $^{+0.1}_{-0.2}$	...	...	$5.83^{6.22}_{4.82}$
104419.63−591658.6	$96.4^{107}_{86.4}$	7.88e-6	1.38	2.05	5	0.38	15.5 $^{+5.8}_{...}$	2.3 $^{+1.2}_{-0.7}$	54.1 $^{+0.08}_{-0.09}$	...	...	$1.54^{1.82}_{1.09}$
104422.51−593925.4	198.4^{214}_{183}	6.38e-6	1.34	1.13	6	0.26	21.9 $^{+0.2}_{-0.5}$	0.43 $^{+0.2}_{-0.3}$	54.4 $^{+0.5}_{-0.5}$	3.3	53.8 $^{+0.3}_{-0.4}$	$1.29^{1.36}_{0.312}$
104422.91−595935.9	$4169.9^{4.24E+03}_{4.11E+03}$	3.19e-4	1.15	0.71	74	0.35	19.4 $^{+1.8}_{...}$	0.63 $^{+0.03}_{-0.04}$	55.5 $^{+0.21}_{-0.02}$	1.6 $^{+0.2}_{-0.1}$	55.3 $^{+0.05}_{-0.10}$	$56.5^{57.8}_{48.9}$
104429.47−595718.1	124.2^{136}_{112}	9.73e-6	0.91	0.94	5	0.31	21.0 $^{+0.7}_{...}$	0.30 $^{+0.2}_{-0.1}$	54.6 $^{+1.0}_{-0.4}$	...	...	$1.56^{1.68}_{0.}$
104430.34−593726.8	395.4^{417}_{374}	1.29e-5	1.37	0.95	16	0.38	21.4 $^{+0.3}_{...}$	0.43 $^{+0.15}_{-0.09}$	54.3 $^{+0.3}_{-0.5}$	4.0 $^{...}_{-1.4}$	54.1 $^{+0.1}_{-0.2}$	$2.88^{2.93}_{1.29}$

Table 2
(Continued)

CXOGNC J	Net Counts (counts)	Photon Flux (photons cm^{-2} s^{-1})	Med. En. (keV)	χ^2_ν	dof	$N_{\rm H}$(ISM) (10^{22} cm^{-2})	log($N_{\rm H}$)	kT_1 (keV)	log EM$_1$	kT_2 (keV)	log EM$_2$	Total Obs. Flux (10^{-14} erg cm^{-2} s^{-1})
104432.34−594431.0	310.8^{331}_{291}	2.83e-5	0.97	0.78	11	0.27	$21.6^{+0.2}_{-0.3}$	$0.30^{+0.10}_{-0.07}$	$55.2^{+0.5}_{-0.4}$	...	...	$3.73^{3.93}_{0.52}$
104433.74−594415.4	$1465.1^{1.5E+03}_{1.43E+03}$	1.36e-4	1.03	0.74	27	0.25	$21.6^{+0.2}_{-0.2}$	$0.30^{+0.04}_{-0.05}$	$55.9^{+0.1}_{-0.3}$	$1.1^{+0.9}_{-0.3}$	$54.7^{+0.2}_{-0.4}$	$22.4^{23.3}_{14.4}$
104436.23−600529.0	821.0^{851}_{792}	3.62e-5	1.00	1.51	31	0.28	$21.6^{+0.1}_{-0.2}$	$0.24^{+0.04}_{-0.03}$	$55.7^{+0.2}_{-0.3}$	2.2	$53.9^{+0.2}_{-0.4}$	$6.5^{6.81}_{3.45}$
104436.73−594729.5	$68.9^{77.5}_{60.4}$	4.42e-6	1.07	0.73	5	0.50	$22.0^{+0.2}_{-0.6}$	$0.15^{+0.23}_{-0.03}$	56.3	...	...	$0.50^{0.52}_{0.}$
104437.47−593255.3	343.7^{363}_{325}	2.65e-5	0.94	0.71	14	0.25	$21.3^{+0.3}_{...}$	$0.30^{...}_{-0.06}$	$55.0^{+0.2}_{-0.2}$	4.5	$53.5^{+0.4}_{-0.5}$	$4.76^{5.05}_{2.55}$
104441.80−594656.4	$976.0^{1.01E+03}_{945}$	5.76e-5	1.04	0.89	45	0.35	$21.6^{+0.2}_{-0.2}$	$0.28^{+0.05}_{-0.06}$	$55.6^{+0.2}_{-0.3}$	$1.8^{+1.6}_{-0.6}$	$54.2^{+0.2}_{-0.3}$	$8.18^{8.44}_{3.64}$
104443.88−592125.1	183.8^{197}_{170}	1.41e-5	1.00	0.82	8	0.24	$21.5^{+0.4}_{-1.5}$	$0.46^{+0.2}_{-0.2}$	$54.5^{+0.7}_{-0.4}$	...	...	$2.01^{2.29}_{0.30}$
104445.04−593354.6	$9275.1^{9.37E+03}_{9.18E+03}$	1.01e-3	1.28	0.97	128	0.30	$21.7^{+0.06}_{-0.07}$	$0.31^{+0.02}_{-0.01}$	$56.6^{+0.1}_{-0.1}$	$2.3^{+0.2}_{-0.2}$	$56.0^{+0.02}_{-0.03}$	$169.^{173.}_{162.}$
104445.27−595441.5	378.5^{400}_{357}	1.64e-5	1.07	1.20	15	0.34	$21.5^{+0.2}_{-0.3}$	$0.61^{+0.14}_{-0.06}$	$54.5^{+0.1}_{-0.1}$	...	...	$2.3^{2.45}_{2.02}$
104447.31−594353.3	$108.4^{119}_{97.7}$	3.63e-5	1.01	0.55	5	0.25	$21.6^{+0.1}_{-0.6}$	$0.53^{+0.2}_{-0.2}$	$54.6^{+0.5}_{-0.3}$	...	...	$2.39^{2.46}_{0.}$
104454.06−594129.4	173.1^{186}_{160}	8.50e-6	1.54	0.59	7	0.29	$21.0^{+0.6}_{...}$	$2.9^{+1.7}_{-0.9}$	$54.1^{+0.12}_{-0.10}$	...	...	$2.05^{2.35}_{1.6}$
104454.70−595601.8	309.4^{329}_{290}	1.22e-5	1.28	0.79	11	0.33	$15.2^{+6.1}_{...}$	$0.59^{+0.1}_{-0.3}$	$53.9^{+0.2}_{-0.1}$	$5.4^{...}_{-2.3}$	$54.0^{+0.1}_{-0.1}$	$2.89^{3.08}_{1.43}$
104504.75−594053.7	281.2^{302}_{261}	1.53e-5	1.57	1.04	11	0.20	$21.0^{+0.6}_{...}$	$2.7^{+1.2}_{-0.7}$	$54.3^{+0.12}_{-0.09}$	...	...	$3.3^{3.82}_{2.46}$
104505.79−594519.7	204.9^{219}_{191}	1.11e-5	1.06	0.73	8	0.47	$21.7^{+0.2}_{-0.4}$	$0.32^{+0.17}_{-0.10}$	$55.0^{+0.6}_{-0.5}$	...	...	$1.44^{1.54}_{0.}$
104505.84−594307.7	102.2^{112}_{92}	2.71e-5	1.07	0.63	5	0.36	$21.4^{+0.3}_{...}$	$0.70^{+0.2}_{-0.1}$	$54.3^{+0.3}_{...}$	...	...	$1.6^{1.79}_{0.90}$
104505.90−594006.0	$1654.0^{1.7E+03}_{1.61E+03}$	8.27e-5	1.00	1.22	58	0.28	$21.5^{+0.1}_{-0.1}$	$0.18^{+0.04}_{-0.03}$	$55.8^{+0.3}_{-0.3}$	0.54	$55.1^{+0.05}_{-0.06}$	13.2
104506.70−594156.6	91.8^{102}_{82}	4.45e-6	0.93	0.99	5	0.31	$18.4^{+3.3}_{...}$	$0.36^{+0.1}_{-0.1}$	$54.0^{+0.9}_{-0.2}$	...	...	$0.70^{0.68}_{0.}$
104508.21−594049.6	$65.5^{74.3}_{56.8}$	3.75e-6	1.07	0.23	3	0.22	$21.7^{+0.4}_{...}$	$0.20^{+0.4}_{...}$	$54.8^{+0.6}_{-8.0}$	$2.5^{...}_{-1.0}$	$53.4^{+0.2}_{-0.5}$	$0.71^{0.72}_{0.19}$
104508.23−594607.0	$1909.4^{1.95E+03}_{1.87E+03}$	9.60e-5	1.55	0.94	94	0.56	$21.6^{+0.2}_{-0.5}$	$0.76^{+0.2}_{-0.2}$	$54.9^{+0.3}_{-0.5}$	$2.1^{+0.3}_{-0.2}$	$55.2^{+0.05}_{-0.08}$	$19.8^{20.8}_{18.4}$
104512.23−594500.5	204.9^{219}_{190}	2.68e-5	1.18	1.25	6	0.37	$21.1^{+0.4}_{...}$	$0.70^{+0.13}_{-0.09}$	$54.4^{+0.2}_{-0.2}$	11.	$53.9^{+0.2}_{-0.3}$	$4.71^{5.58}_{1.08}$
104512.72−594446.2	384.1^{404}_{364}	1.90e-5	1.04	0.84	18	0.38	$21.2^{+0.3}_{-1.0}$	$0.60^{+0.07}_{-0.08}$	$54.5^{+0.1}_{-0.1}$	...	...	$2.7^{2.86}_{2.34}$
104512.88−594419.3	579.7^{604}_{556}	2.86e-5	1.09	0.88	26	0.44	$21.4^{+0.2}_{-0.3}$	$0.63^{+0.07}_{-0.05}$	$54.8^{+0.1}_{-0.1}$	...	...	$3.98^{4.28}_{3.63}$
104516.52−594337.1	624.4^{650}_{599}	3.13e-5	1.12	0.98	27	0.43	$21.8^{+0.1}_{-0.2}$	$0.32^{+0.08}_{-0.05}$	$55.5^{+0.2}_{-0.4}$	$1.6^{...}_{-0.8}$	$54.0^{+0.4}_{-0.7}$	$4.41^{4.59}_{2.67}$
104520.57−594251.1	$77.1^{86.2}_{68.1}$	6.77e-6	0.97	0.49	5	0.31	$21.6^{+0.4}_{...}$	$0.32^{+0.3}_{-0.1}$	$54.5^{+1.3}_{-0.7}$	...	...	$0.76^{0.76}_{0.}$
104534.04−595726.7	164.4^{177}_{152}	9.97e-6	1.03	1.23	6	0.45	$21.8^{+0.2}_{-0.9}$	$0.23^{+0.23}_{-0.06}$	$55.4^{+0.8}_{-8.6}$	...	...	$1.34^{1.32}_{0.}$
104536.33−594823.5	$69.0^{78.6}_{59.5}$	5.21e-6	1.26	0.60	5	0.79	$21.4^{+0.6}_{...}$	$0.50^{+0.3}_{-0.3}$	$54.4^{+1.6}_{-0.4}$	...	...	$0.67^{0.70}_{0.}$
104544.13−592428.1	$19161.0^{1.93E+04}_{1.9E+04}$	8.08e-4	1.23	1.52	185	0.31	$21.5^{+0.06}_{-0.07}$	$0.62^{+0.02}_{-0.01}$	$56.0^{+0.06}_{-0.06}$	$1.6^{+0.06}_{-0.05}$	$55.8^{+0.02}_{-0.03}$	$135.^{137.}_{133.}$
104553.71−595703.9	$78.1^{87.3}_{69}$	6.17e-6	1.53	0.21	5	0.47	$17.4^{+4.4}_{...}$	$2.4^{+1.3}_{-1.0}$	$54.0^{+0.21}_{-0.10}$	...	...	$1.35^{1.59}_{0.90}$
104605.70−595049.5	544.6^{569}_{520}	2.18e-5	1.12	0.90	23	0.58	$21.7^{+0.1}_{-0.4}$	$0.33^{+0.19}_{-0.05}$	$55.4^{+0.3}_{-0.5}$	...	...	$2.87^{2.98}_{1.28}$
104622.02−600118.8	160.1^{174}_{147}	5.99e-6	1.83	0.72	6	0.21	$20.9^{+0.8}_{...}$	$16.^{...}_{-10.3}$	$53.9^{+0.07}_{-0.09}$	...	...	$2.25^{2.73}_{0.002}$
104622.48−595320.4	492.7^{516}_{470}	1.81e-5	1.25	1.47	23	0.52	$21.8^{+0.09}_{-0.11}$	$0.55^{+0.06}_{-0.06}$	$54.9^{+0.1}_{-0.1}$	...	...	$2.48^{2.64}_{2.19}$
104633.07−600412.9	162.7^{176}_{149}	6.79e-6	1.00	0.56	6	0.34	$21.1^{+0.6}_{...}$	$0.48^{+0.1}_{-0.2}$	$54.2^{+0.6}_{-0.2}$	...	...	$1.03^{1.15}_{0.15}$
104635.70−593700.7	158.0^{172}_{144}	9.53e-6	1.25	0.24	3	0.46	$17.7^{+4.2}_{...}$	$0.74^{+0.2}_{...}$	$53.8^{+0.5}_{-7.0}$	$2.0^{...}_{-0.8}$	$53.8^{+0.4}_{-0.9}$	$1.43^{1.58}_{0.69}$
104653.84−600441.9	$56.6^{64.3}_{49.1}$	5.66e-6	1.03	0.88	5	0.32	$21.7^{+0.5}_{...}$	$0.34^{+0.4}_{...}$	$54.5^{...}_{-0.8}$	...	...	$0.65^{0.67}_{0.}$
104712.63−600550.8	502.1^{525}_{480}	3.66e-5	1.22	0.91	24	0.43	$21.8^{+0.08}_{-0.10}$	$0.56^{+0.07}_{-0.06}$	$55.2^{+0.1}_{-0.1}$	...	...	$4.96^{5.35}_{4.4}$
104716.41−600539.9	$51.7^{58.9}_{44.4}$	3.80e-6	1.16	0.37	5	0.41	$21.7^{+0.4}_{-1.1}$	$0.54^{+0.4}_{-0.3}$	$54.2^{+1.4}_{-0.5}$	...	...	$0.52^{0.58}_{0.}$
104815.50−601556.9	$84.0^{93.3}_{74.8}$	6.69e-6	1.03	1.29	5	0.49	$21.1^{+0.9}_{...}$	$0.54^{+0.2}_{-0.3}$	$54.2^{+1.6}_{-0.2}$	...	...	$0.91^{0.89}_{0.}$
104837.74−601325.7	668.9^{695}_{643}	8.53e-5	1.00	0.94	26	0.19	$21.5^{+0.2}_{-0.7}$	$0.31^{+0.08}_{-0.05}$	$55.5^{+0.2}_{-0.5}$	$1.4^{+1.3}_{-0.3}$	$54.4^{+0.2}_{-0.3}$	$12.3^{12.8}_{8.32}$
104924.95−594944.0	$82.4^{91.6}_{73.2}$	6.62e-6	0.91	1.11	6	0.34	$21.5^{+0.3}_{...}$	$0.23^{+0.20}_{-0.09}$	$55.0^{+1.2}_{...}$	...	...	$1.04^{1.15}_{0.}$
104557.13−595643.1	$500.^{523.}_{478.}$	3.05e-5	1.61	0.70	26		$22.2^{+0.0}_{-0.2}$	$0.24^{+0.21}_{-0.07}$	$56.0^{+0.8}_{-1.2}$	$2.6^{+1.0}_{-0.6}$	$54.8^{+0.1}_{-0.1}$	$7.92^{8.35}_{5.15}$
Stacked O stars		2.34e-6		0.24	8	0.26	$21.2^{21.6}_{...}$	$0.36^{0.59}_{0.22}$	$53.8^{54.7}_{...}$	...	...	0.37
Stacked B stars		1.32e-6		1.78	23	0.22	$21.6^{21.7}_{21.6}$	$0.28^{0.38}_{0.21}$	$53.9^{54.1}_{53.4}$	$2.27^{4.56}_{1.52}$	$52.9^{53.0}_{52.7}$	0.23

Notes. Indices and exponents provides the lower and upper limits of the confidence interval (with 68% confidence for counts and 90% confidence for the spectral parameters and fluxes). Source 104557.13−595643.1 corresponds to the star Cl* Trumpler 16 MJ 640 (or Hen 3-485 or SS73_24), which is of type Be pec. Without precise knowledge of its photometry and other properties, its bolometric luminosity and its interstellar column could not be derived, which is why this source was not considered further. It is only shown here for completeness. For more details on the stacked objects, see Section 7.

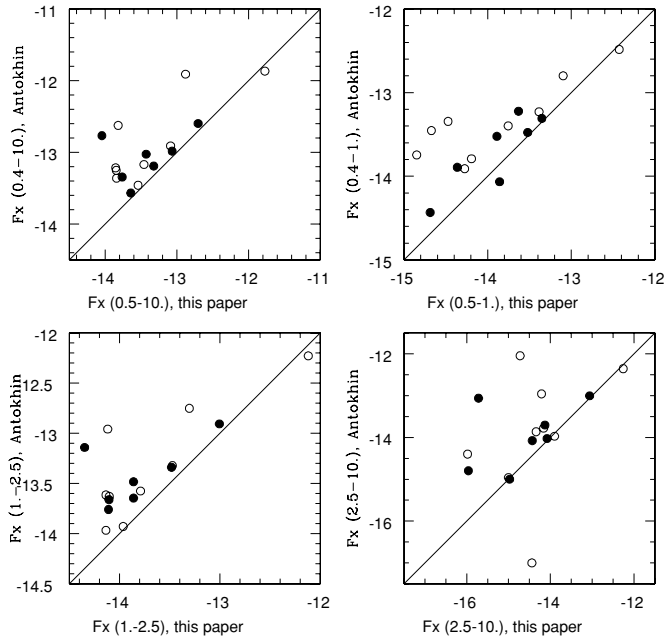

Figure 2. Comparison of the observed (absorbed) fluxes between Antokhin et al. (2008) and this paper. Filled circles correspond to X-ray sources with companions within 5″ and open circles to isolated X-ray sources.

necessary, and there appears to be a significant additional (circumstellar) absorbing column of about 4×10^{21} cm^{-2}. When two temperatures are needed to fit a spectrum, the hotter component is of reduced strength compared to the main, "cool" component. Note that the value of the additional absorbing column does not show any dependence on the bolometric luminosity of the associated star. For B-type stars, no additional absorbing column is needed, but the dominant temperatures are higher.

Due to their high count rates, photon pile-up may affect four sources in the O and early-B population (Broos et al. 2011): HD 93129A, HD 93205, HD 93206, and HD 93250. We ignore the mild pile-up of HD 93403. In this paper, the spectral fitting for these sources was performed on reconstructed spectra (see Broos et al. for details on the reconstruction method). Additional fittings performed on individual X-ray spectra of these bright objects are presented in Parkin et al. (2011, QZ Car) and Gagné et al. (2011, other massive stars).

2.2. Comparison with Previous Studies

Ten sources are in common with the *Chandra* analysis reported by Evans et al. (2004); except for the two known variable stars (HD 93250, see Rauw et al. 2009, and Tr16 MJ 496, described below), their observed fluxes agree with ours to within the errors (which are of the order 10%–20%). For completeness, we can also compare our results with the *XMM-Newton* study of Antokhin et al. (2008). Sixteen of their stars (excluding the O+OB binaries and close pairs such as HD 93129AB and HD 93161AB) are in common with our survey. However, there is not an exact one-to-one scaling when comparing the observed fluxes of these sources (see Figure 2). This difference appears especially important for three objects: HD 303308 (O4V), Tr14 MJ 127 (O9V), and Tr14 MJ 181 (B1.5V). These flux differences may be explained in several ways: energy band boundaries, crowding, variability, and exposure lengths. First, Antokhin et al. (2008) use a soft boundary of 0.4 keV while we used 0.5 keV. This can explain why Antokhin's fluxes are systematically higher than ours (but this cannot explain a factor of two difference). Also, *Chandra*, which has better spatial resolution than *XMM-Newton*, can distinguish close neighbors more easily, again making the *XMM-Newton* X-ray luminosities systematically overestimated. For example, HD 93129AB was seen as a single source in *XMM-Newton*, while the two components are here clearly separated, with additional, fainter close companions detected. However, crowding is not the only cause for the difference, as sources without any detectable companions are still much more luminous in Antokhin's data (e.g., HD 303308, Tr14 MJ 181). Variability may also cause brightness differences. If the X-ray emission of the B-star Tr14 MJ 181 is magnetic in origin (X-rays from a PMS companion or a corona intrinsic to the star), flares should be quite common, though none are detected in our data. Finally, the exposure and sensitivities are quite different in the *XMM-Newton* and *Chandra* data sets. On average, the exposure and sensitivity were lower for *Chandra*; the low number of counts certainly explains the scatter of the hard flux (in the 2.5–10.0 keV band) but this can also be true for a few particularly faint objects (e.g., Tr14 MJ 127, LS 1897). There is thus no single explanation for the observed flux differences between Antokhin's work and ours.

Comparing the final X-ray luminosities (corrected for interstellar absorption) and the associated L_X–L_{BOL} ratios to the values from Antokhin et al. (2008) is even more complicated. First, the interstellar columns are different, as we did not choose the same gas-to-dust ratio and R_V; with a larger assumed distance (increasing luminosities by 20%) and interstellar columns increasing by 15% in Antokhin et al. because of the changed gas-to-dust ratio alone, the absolute values of the absorption-corrected X-ray luminosities from Antokhin et al. are expected to differ from our values. Second, the bolometric luminosities were derived in a very different way, also leading to differences. As a result, Antokhin et al. find an average $\log(L_X/L_{BOL}) = -6.58$, i.e., a value larger by about 0.7 dex compared to that derived from our data (see the next section).

It is interesting to note that, using $R_V = 3.1$ and deriving the bolometric luminosities from V magnitudes, our data yield $\log(L_X/L_{BOL}) = -6.99$. The choice of a given calibration therefore clearly affects the absolute value of the L_X–L_{BOL} ratio and one should not simply compare the values of these ratios given in different studies. Only homogeneous studies of global samples, such as done in Berghöfer et al. (1997) or Nazé (2009), can be used for such purposes. However, as our data set is homogeneous in itself (same instrument and similar completeness limit throughout the field of view), its results can be seen as self-consistent and a comparison between different objects studied in this paper is feasible.

3. THE L_X–L_{BOL} RELATION

Table 3 summarizes the main properties of the brightest sources (those with >50 recorded counts). The first two columns give the X-ray source name and the stellar identification. They are followed by the spectral type (Column 3), the binary status (Column 4), the bolometric luminosity (Column 5; Columns 2–5 are reproduced from the stellar catalog by Povich et al. 2011; Gagné et al. 2011), the X-ray luminosities in four energy bands (defined below, Columns 6–9), and the L_X–L_{BOL} ratios in the same energy bands (Columns 10–13). Note that the X-ray luminosities were corrected by the interstellar absorption only (this enables us to compare the actual X-ray throughput of massive stars and eases the comparison with other studies, as the circumstellar absorption is not always taken into account in

Table 3
Summary of Sources' Properties

CXOGNC J	Name	Sp. Type	Bin?	$\log(L_{BOL}/L_{\odot})$	$\log(L_X)$				$\log(L_X/L_{BOL})$			
					Total	Soft	Medium	Hard	Total	Soft	Medium	Hard
104012.42−594810.1	HD 92607	O8 V		5.21	31.75	31.61	31.16	30.14	−7.04	−7.19	−7.63	−8.66
104031.71−594643.9	HD 92644	B1.5 III		4.36	31.12	31.00	30.52	28.00	−6.82	−6.95	−7.42	−9.94
104210.35−595800.9	HD 305439A	B0 Ia		5.17	31.11	30.96	30.56	29.06	−7.64	−7.79	−8.18	−9.69
104243.71−595416.6	HD 305438	O8 V((f))		4.76	31.19	31.05	30.32	30.32	−7.16	−7.30	−8.03	−8.02
104311.17−594420.8	HD 303316	O6 V		5.14	31.53	31.43	30.85	28.58	−7.20	−7.30	−7.88	−10.15
104315.33−601204.3	HD 93028	O9 V		4.86	31.23	31.19	30.18	25.80	−7.22	−7.26	−8.27	−12.65
104317.92−600803.1	HD 93027	O9.5 V		4.81	31.08	31.01	30.26	27.72	−7.31	−7.38	−8.13	−10.67
104341.24−593548.1	LS 1809	O7 V		5.03	31.03	30.76	30.69	29.05	−7.58	−7.86	−7.92	−9.56
104343.42−602027.7	HD 305556	B0 Ib		4.95	31.17	31.12	30.22	27.77	−7.36	−7.41	−8.30	−10.76
104343.55−593403.4	Cl* Trumpler 14 MJ 99	B2 V		3.64	31.25	30.58	30.87	30.83	−5.97	−6.65	−6.36	−6.40
104343.99−594817.9	HD 305518	O9.5 V		4.97	31.27	31.18	30.40	29.87	−7.29	−7.37	−8.15	−8.69
104345.04−595325.0	Cl* Trumpler 14 MJ 126	B2 V		3.80	31.04	30.44	30.73	30.47	−6.34	−6.94	−6.65	−6.92
104346.69−593254.7	Cl* Trumpler 14 MJ 115	O6 V		5.17	31.71	31.64	30.85	29.84	−7.04	−7.11	−7.89	−8.91
104348.70−593324.2	Cl* Trumpler 14 MJ 127	O9 V		4.64	31.13	30.95	30.63	29.10	−7.10	−7.27	−7.59	−9.12
104353.63−593328.4	Cl* Trumpler 14 MJ 150	O9 V		4.45	30.98	30.63	30.70	29.58	−7.05	−7.41	−7.34	−8.46
104354.40−593257.4	HD 93128	O3.5 V((f+))		5.63	32.11	31.96	31.58	29.70	−7.10	−7.25	−7.63	−9.51
104355.36−593248.8	Cl* Trumpler 14 MJ 165	O8 V		5.01	31.44	31.38	30.57	27.54	−7.15	−7.21	−8.02	−11.05
104357.47−593251.3	HD 93129A	O2 If*	Y	6.18	32.80	32.29	32.57	31.85	−6.97	−7.48	−7.20	−7.92
104357.46−600528.3	LS 1821	O8.5 V		4.68	31.25	31.19	30.39	28.05	−7.01	−7.07	−7.87	−10.21
104357.65−593253.7	HD 93129B	O3.5 V((f+))		5.53	32.03	31.91	31.41	29.76	−7.08	−7.20	−7.70	−9.35
104357.96−593353.4	Cl* Trumpler 14 MJ 181	B1.5 V		3.80	31.13	30.51	30.80	30.60	−6.25	−6.87	−6.58	−6.78
104358.45−593301.5	Cl* Trumpler 14 MJ 184	B1 V		4.03	31.09	30.52	30.63	30.68	−6.52	−7.10	−6.99	−6.93
104359.92−593225.4	Cl* Trumpler 14 MJ 192	O6.5 V		5.10	31.48	31.42	30.52	27.78	−7.21	−7.26	−8.17	−10.90
104400.17−600607.7	Cl Collinder 228 68	B1 Vn		3.95	31.07	30.28	30.72	30.67	−6.46	−7.25	−6.81	−6.86
104400.16−600509.8	HD 93146	O6.5 V		5.26	31.77	31.67	31.09	28.57	−7.08	−7.18	−7.76	−10.28
104400.38−595227.5	HD 93130	O6 III		5.68	31.65	31.47	31.16	29.81	−7.61	−7.79	−8.11	−9.45
104405.09−593341.4	Cl* Trumpler 14 MJ 218	B1.5 V		3.95	30.92	30.27	30.55	30.46	−6.62	−7.27	−6.98	−7.08
104405.84−593511.6	Cl* Trumpler 14 MJ 224	B1 V		4.15	31.16	30.49	30.81	30.68	−6.58	−7.25	−6.92	−7.05
104407.26−593430.5	HD 93160	O6 III		5.70	32.10	31.97	31.45	30.73	−7.19	−7.32	−7.84	−8.55
104408.84−593434.4	HD 93161A	O8 V + O9 V	Y	5.28	31.94	31.80	31.33	30.54	−6.92	−7.07	−7.53	−8.32
104409.08−593435.3	HD 93161B	O6.5 V(f)		5.43	31.75	31.55	31.30	29.80	−7.27	−7.46	−7.72	−9.21
104411.04−600321.8	HD 305536	O9.5 V		4.83	31.25	30.91	30.81	30.53	−7.16	−7.50	−7.61	−7.88
104413.19−594310.1	Cl* Trumpler 16 MJ 257	O3/4 If		5.42	31.80	31.09	31.66	30.69	−7.21	−7.92	−7.35	−8.31
104419.63−591658.6	HD 93190	B0 IV:ep		5.39	31.13	30.49	30.78	30.65	−7.84	−8.48	−8.19	−8.32
104422.51−593925.4	Cl* Trumpler 16 MJ 289	B1.5 V		3.77	31.01	30.37	30.66	30.51	−6.35	−6.98	−6.69	−6.84
104422.91−595935.9	QZ Car	O9.7Ib:(n)+b2v+B0Ib+o9v	Y	6.23	32.82	32.57	32.39	31.69	−6.99	−7.24	−7.43	−8.13
104429.47−595718.1	HD 305523	O9 II		5.24	31.41	31.34	30.59	28.27	−7.42	−7.49	−8.24	−10.55
104430.34−593726.8	Cl* Trumpler 16 MJ 327	B0 V		4.84	31.45	31.02	30.97	30.91	−6.98	−7.41	−7.46	−7.52
104432.34−594431.0	HD 93204	O5.5 V((fc))		5.39	31.67	31.55	31.07	28.85	−7.30	−7.42	−7.90	−10.12
104433.74−594415.4	HD 93205	O3.5 V + O8 V	Y	5.79	32.40	32.23	31.89	30.67	−6.97	−7.14	−7.48	−8.71

Table 3
(Continued)

CXOGNC J	Name	Sp. Type	Bin?	$\log(L_{BOL}/L_{\odot})$	$\log(L_X)$				$\log(L_X/L_{BOL})$			
					Total	Soft	Medium	Hard	Total	Soft	Medium	Hard
104436.23−600529.0	HD 93222	O7 III		5.46	31.94	31.82	31.24	30.48	−7.11	−7.23	−7.81	−8.57
104436.73−594729.5	Cl* Trumpler 16 MJ 359	O8 V		4.86	30.97	30.83	30.42	26.94	−7.47	−7.62	−8.02	−11.50
104437.47−593255.3	HD 303311	O5 V		5.15	31.77	31.66	31.06	30.38	−6.96	−7.07	−7.67	−8.36
104441.80−594656.4	Cl* Trumpler 16 MJ 380	O6 V		5.50	32.06	31.90	31.48	30.65	−7.02	−7.18	−7.60	−8.43
104443.88−592125.1	HD 93249	O9 III		5.11	31.33	31.15	30.86	29.21	−7.36	−7.54	−7.83	−9.49
104445.04−593354.6	HD 93250	O4 III(fc)		5.95	33.19	32.76	32.78	32.55	−6.35	−6.77	−6.75	−6.98
104445.27−595441.5	HD 305524	O7 V((f))		5.12	31.43	31.20	31.02	29.73	−7.28	−7.51	−7.69	−8.98
104447.31−594353.3	Cl* Trumpler 16 MJ 408	O7 V((f))+O9.5 V+B0.2 IV	Y	5.09	31.38	31.15	30.99	29.53	−7.29	−7.52	−7.68	−9.14
104454.06−594129.4	Cl* Trumpler 16 MJ 427	B1 V		4.03	31.19	30.37	30.81	30.84	−6.42	−7.24	−6.81	−6.78
104454.70−595601.8	Cl* Trumpler 14 MJ 449	O8.5 V((f))		4.74	31.44	31.06	30.89	30.91	−6.89	−7.27	−7.43	−7.41
104504.75−594053.7	Cl Trumpler 16 64	B1.5 Vb		3.85	31.38	30.58	31.01	31.01	−6.05	−6.85	−6.42	−6.42
104505.79−594519.7	Cl* Trumpler 16 MJ 484	O9 III	Y	5.06	31.38	31.19	30.91	28.85	−7.27	−7.45	−7.73	−9.80
104505.84−594307.7	Cl* Trumpler 16 MJ 481	O9.5 V	Y	4.86	31.27	31.01	30.88	29.70	−7.17	−7.43	−7.56	−8.74
104505.90−594006.0	HD 303308	O4 V((fc))	Y	5.57	32.26	32.14	31.62	30.09	−6.90	−7.01	−7.53	−9.06
104506.70−594156.6	Cl* Trumpler 16 MJ 488	O8.5 V		4.64	31.04	30.96	30.27	28.17	−7.19	−7.27	−7.96	−10.06
104508.21−594049.6	Cl* Trumpler 16 MJ 493	O9.5 V+B0.3 V	Y	4.60	30.88	30.69	30.21	29.99	−7.30	−7.49	−7.97	−8.20
104508.23−594607.0	Cl* Trumpler 16 MJ 496	O8.5 V		4.97	32.26	31.52	31.96	31.75	−6.30	−7.04	−6.59	−6.80
104512.23−594500.5	HD 93343	O8 V + O7-8.5 V	Y	5.06	31.68	31.33	31.19	31.04	−6.96	−7.31	−7.46	−7.61
104512.72−594446.2	Cl* Trumpler 16 MJ 516	O7.5 V + O9 V	Y	5.21	31.56	31.38	31.08	29.70	−7.23	−7.42	−7.72	−9.09
104512.88−594419.3	Cl* Trumpler 16 MJ 517	O7 V+ O8 V+ O9 V	Y	5.40	31.74	31.52	31.32	30.03	−7.25	−7.47	−7.67	−8.96
104516.52−594337.1	Cl* Trumpler 16 MJ 535	O5.5-6 V +B2 V-III	Y	5.51	31.78	31.53	31.38	30.31	−7.31	−7.56	−7.71	−8.78
104520.57−594251.1	Cl* Trumpler 16 MJ 554	O9.5 V		4.63	31.01	30.87	30.44	28.32	−7.20	−7.34	−7.77	−9.90
104534.04−595726.7	HD 305532	O6 V		5.15	31.39	31.27	30.79	28.26	−7.34	−7.46	−7.94	−10.47
104536.33−594823.5	FO 15	O5.5 Vz + O9.5 V	Y	5.31	31.24	31.05	30.78	29.22	−7.65	−7.84	−8.11	−9.67
104544.13−592428.1	HD 93403	O5.5 I+ O7 V	Y	5.95	33.11	32.72	32.79	32.18	−6.42	−6.81	−6.74	−7.35
104553.71−595703.9	Cl* Trumpler 16 MJ 632	O9.5 V		4.60	31.09	30.45	30.73	30.62	−7.09	−7.74	−7.45	−7.56
104605.70−595049.5	HD 305525	O4 V		5.59	31.76	31.57	31.30	29.26	−7.42	−7.61	−7.87	−9.92
104622.02−600118.8	HD 93501	B1.5 III:		4.49	31.19	30.09	30.56	31.02	−6.88	−7.98	−7.51	−7.05
104622.48−595320.4	Cl* Trumpler 14 MJ 691	O5 V		5.29	31.53	31.20	31.24	29.90	−7.35	−7.68	−7.64	−8.98
104633.07−600412.9	HD 305539	O7		4.90	31.16	31.02	30.60	28.94	−7.33	−7.47	−7.88	−9.55
104635.70−593700.7	HD 303304	O7 V		5.28	31.23	30.90	30.83	30.37	−7.64	−7.97	−8.04	−8.49
104653.84−600441.9	HD 93576	O9 IV		4.83	30.91	30.72	30.45	28.43	−7.50	−7.69	−7.96	−9.98
104712.63−600550.8	HD 93632	O5 III(f)		5.87	31.77	31.43	31.49	30.20	−7.68	−8.02	−7.96	−9.25
104716.41−600539.9	HD 305612	O9 V		4.87	30.80	30.50	30.48	29.10	−7.65	−7.95	−7.97	−9.35
104815.50−601556.9	HD 305619	O9.7 Ib		5.30	31.20	31.04	30.67	29.13	−7.68	−7.84	−8.21	−9.76
104837.74−601325.7	HD 93843	O5 III(fc)		5.64	32.08	31.90	31.56	30.65	−7.14	−7.32	−7.66	−8.57
104924.95−594944.0	HD 305599	B0 Ib		4.64	31.28	31.22	30.42	27.76	−6.94	−7.01	−7.81	−10.47

Note. The X-ray luminosities have been corrected for the interstellar absorption only (see the text).

Table 4
$\log(L_X/L_{BOL})$ Ratio

Group of Objects	N	0.5–10. keV	0.5–1. keV	1.–2.5 keV	2.5–10. keV
O stars					
All, single	45	-7.22 ± 0.28	-7.42 ± 0.28	-7.79 ± 0.33	-9.30 ± 1.17
>100 counts, single	29	-7.18 ± 0.30	-7.41 ± 0.28	-7.72 ± 0.35	-9.00 ± 1.02
50–100 counts, single	16	-7.28 ± 0.23	-7.45 ± 0.28	-7.91 ± 0.26	-9.85 ± 1.25
All, single exc.	43	-7.26 ± 0.21	-7.45 ± 0.26	-7.84 ± 0.23	-9.41 ± 1.07
>100 counts, single exc.	27	-7.24 ± 0.20	-7.45 ± 0.25	-7.80 ± 0.21	-9.15 ± 0.87
All, binaries	15	-7.11 ± 0.28	-7.35 ± 0.26	-7.57 ± 0.32	-8.63 ± 0.71
>100 counts, binaries	13	-7.05 ± 0.25	-7.30 ± 0.23	-7.49 ± 0.27	-8.59 ± 0.69
50–100 counts, binaries	2	-7.48 ± 0.24	-7.66 ± 0.25	-8.04 ± 0.10	-8.93 ± 1.04
All, binaries exc.	14	-7.16 ± 0.21	-7.39 ± 0.22	-7.63 ± 0.23	-8.72 ± 0.63
>100 counts, binaries exc.	12	-7.10 ± 0.16	-7.34 ± 0.18	-7.56 ± 0.16	-8.69 ± 0.61
All, single exc., I	2	-7.45 ± 0.33	-7.88 ± 0.06	-7.78 ± 0.61	-9.03 ± 1.02
All, single exc., III	6	-7.35 ± 0.25	-7.54 ± 0.31	-7.87 ± 0.15	-8.98 ± 0.46
All, single exc., V	32	-7.21 ± 0.19	-7.40 ± 0.24	-7.82 ± 0.23	-9.46 ± 1.18
Tr16, all single exc.	14	-7.24 ± 0.15	-7.42 ± 0.22	-7.84 ± 0.24	-9.68 ± 1.34
Tr14, all single exc.	6	-7.10 ± 0.06	-7.25 ± 0.10	-7.72 ± 0.28	-9.38 ± 0.83
All, single exc., O2–5.5	9	-7.25 ± 0.22	-7.50 ± 0.33	-7.71 ± 0.18	-9.15 ± 0.65
All, single exc., O6–8	18	-7.26 ± 0.20	-7.41 ± 0.25	-7.89 ± 0.16	-9.49 ± 1.03
>100 counts, single exc., O6–8	13	-7.25 ± 0.20	-7.41 ± 0.24	-7.84 ± 0.16	-9.14 ± 0.79
All, single exc., O8.5–9.7	16	-7.26 ± 0.22	-7.46 ± 0.24	-7.86 ± 0.30	-9.48 ± 1.32
>100 counts, single exc., O8.5–9.7	5	-7.23 ± 0.21	-7.44 ± 0.11	-7.85 ± 0.34	-9.20 ± 1.50
All, single exc., $\log(L_X) > 38.5$	28	-7.28 ± 0.21	-7.46 ± 0.28	-7.85 ± 0.21	-9.38 ± 0.81
All, single exc., $\log(L_X) < 38.5$	15	-7.22 ± 0.20	-7.43 ± 0.23	-7.82 ± 0.28	-9.49 ± 1.48
All, single exc., $\log(L_X) > 38.75$	18	-7.30 ± 0.23	-7.50 ± 0.30	-7.82 ± 0.23	-9.22 ± 0.70
All, single exc., $38.25 < \log(L_X) < 38.75$	20	-7.25 ± 0.20	-7.41 ± 0.24	-7.92 ± 0.20	-9.69 ± 1.31
All, single exc., $\log(L_X) < 38.25$	5	-7.13 ± 0.07	-7.41 ± 0.19	-7.62 ± 0.25	-9.02 ± 1.04
Weak wind stars	8	-7.17 ± 0.21	-7.27 ± 0.24	-7.90 ± 0.25	-9.95 ± 1.34
B stars					
All, single	17	-6.71 ± 0.52	-7.26 ± 0.46	-7.18 ± 0.64	-7.75 ± 1.49
100 counts, single	9	-6.48 ± 0.36	-7.13 ± 0.40	-6.91 ± 0.45	-7.20 ± 1.08
50–100 counts, single	8	-6.96 ± 0.58	-7.41 ± 0.51	-7.49 ± 0.70	-8.38 ± 1.69

Notes. "exc." means without the outliers—the single stars HD 93250, Tr14 MJ 496, and/or the binary HD 93403. Errors correspond to the 1σ dispersion of the data.

the same way). The luminosities are given in the 0.5–10.0 keV ("total"), 0.5–1.0 keV ("soft"), 1.0–2.5 keV ("medium"), and 2.5–10.0 keV ("hard") energy bands. Most of the X-ray emission of massive stars is emitted in the soft and medium bands, the former being more sensitive to absorption effects; the relative strength of these two bands is also an indication of the softness of the emission. Hot stars generally emit few X-rays in the hard band and the corresponding fluxes therefore show large uncertainties. However, this band is useful for detecting peculiar phenomena such as magnetically confined winds or colliding winds (in which cases the hard X-ray flux is enhanced). These phenomena will be explored below.

Averages ($X = \sum X_i/N$) and dispersions ($\sigma = \sqrt{\sum (X_i - X)^2/(N-1)}$) of the $\log(L_X/L_{BOL})$ ratio were evaluated for several different samples of objects. No weighting was applied and comparisons of the means were made following the methods outlined in Lindgren (1968, chapter 7.3) and for a significance level of 1%. Table 4 and Figure 3 summarize the results. We emphasize again that the X-ray luminosities quoted here are corrected only for the interstellar absorbing column and that the hard X-ray fluxes are unreliable due to the small count rates at such high energies for most of our X-ray sources.

3.1. O Stars

As usual, the O-type stars show a clear L_X–L_{BOL} correlation, with similar results regardless of the sample chosen (i.e., >100 counts versus 50–100 counts). Only three stars strongly deviate from the average behavior (Figure 3): HD 93250, HD 93403, and Tr16 MJ 496 (also known as Tr16 22). The first star is a suspected binary, due to the presence of non-thermal radio emission theoretically expected to arise in wind–wind collisions and to the detection of large X-ray variations (Rauw et al. 2009). However, the signature of the companion has never been directly detected (see Rauw et al. 2009, and references therein). The second star is a known binary, whose X-ray emission, monitored by *XMM-Newton*, shows clear signs of a wind–wind collision (see Rauw et al. 2002, for a full analysis of the phenomenon).

The third object was also identified as overluminous (and variable) by Antokhin et al. (2008), and its emission appears quite hard for an O star (see below), suggesting a mechanism other than the usual wind-shock process. In such cases, two possibilities exist: wind–wind collisions and magnetic wind confinement. Although radial velocity variations may have been detected (Combi et al. 2011), the former mechanism is not favored since such a large overluminosity (>1 dex) is neither observed nor theoretically expected in late-type O+OB colliding wind binaries. Tr16 MJ 496 could thus be a magnetic object that might resemble θ^1 Ori C (Gagné et al. 2005); additional spectropolarimetric data and multiwavelength monitoring are needed to confirm this hypothesis. In summary, in all three cases, the detected overluminosities at high energies confirm previous observations and can be explained by X-rays generated in colliding winds or magnetically confined winds in addition to the intrinsic, wind-shock emission.

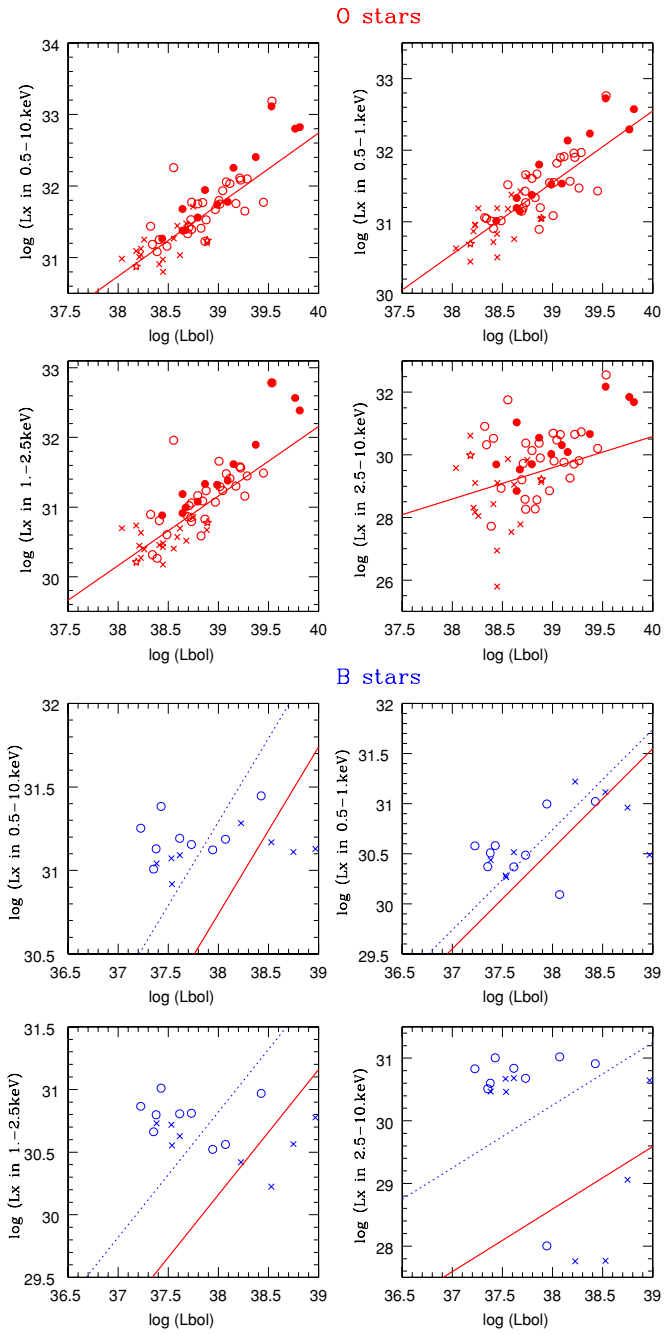

Figure 3. X-ray luminosity in four energy bands as a function of bolometric luminosity, for O stars (upper four panels and lower four panels, in bold red), and B stars (middle four panels and lower four panels, in blue). Open and filled circles refer to singles and binaries, respectively, with >100 counts. Crosses and stars are for singles and binaries recorded with only 50–100 counts. The lines give the L_X–L_{BOL} relation from Table 4 derived for all single O (solid line) and B (dotted line) stars except HD 93250 and Tr14 MJ 496.

(A color version of this figure is available in the online journal.)

Discarding these three sources from the $\log(L_X/L_{BOL})$ average yields a final $\log(L_X/L_{BOL})$ of −7.26 and a dispersion of only 0.2 dex (Table 4), quite similar to that found in NGC 6231 once its two binaries with X-ray-bright wind–wind collisions have been discarded (Sana et al. 2006). This confirms that the L_X–L_{BOL} relationship is quite tight for a homogeneous population of stars; the observed scatter in $\log(L_X/L_{BOL})$ found from large samples (Berghöfer et al. 1997; Nazé 2009) is thus clearly due to the inhomogeneity of the stellar populations in

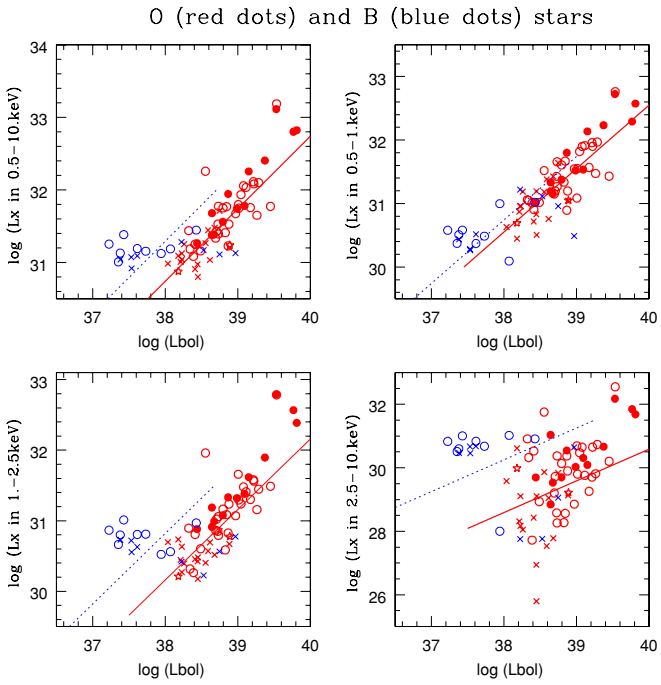

Figure 3. (Continued)

these samples. To study further the L_X–L_{BOL} relationship, we have compared different stellar groups (Table 4). There are no clear, significant differences (at the 1% level) in L_X–L_{BOL} ratios for stars of different luminosity class, as was notably claimed by Albacete Colombo et al. (2007) for Cyg OB2 (considering however that the number of O supergiants is too low for providing statistically meaningful results). Neither were there significant differences (at the 1% level) in L_X–L_{BOL} ratios for stars of different spectral types or of different luminosities (except for the faint versus medium-bright objects in the medium energy band). Compiling single O stars belonging to the clusters Tr14 and Tr16/Cr232 using Cudworth et al. (1993), Table 1 from Walborn (1995), Table 3 from DeGioia-Eastwood et al. (2001), and Tables 5 and 7 from Carraro et al. (2004), a comparison of $\log(L_X/L_{BOL})$ between these two stellar groups can be attempted. Single stars of Tr16 yield very similar results as single stars of the whole Carina region, whereas single stars of Tr14 display a systematically higher $\log(L_X/L_{BOL})$ (as well as smaller dispersions in the total and soft bands) than stars of Tr16 or of the whole area (Table 4). However, the difference in $\log(L_X/L_{BOL})$ is not formally significant (at the 1% level) and only hints at potential differences between clusters, as was already reported in Nazé (2009).

3.2. B Stars

On the other hand, the B stars detected with more than 50 counts show no strong correlation between X-ray and bolometric luminosities (Figure 3) and larger dispersions than for O stars are measured in all bands (Table 4). In all cases, the L_X–L_{BOL} ratios are larger than that of O stars, especially for the medium energy band (e.g., $\log(L_X/L_{BOL}) = -6.9\ldots-7.4$ vs. −7.84 in that band). A possible trend toward higher soft X-ray luminosities for more luminous objects is seen in the soft band (with a similar slope as for O-type stars). In contrast, the medium-band X-ray luminosities appear rather constant, with even a shallow decrease toward higher bolometric luminosities (Figure 3). A similar situation is seen at the highest energies, although there

are now a few outliers (most probably due to the low number of hard photon counts recorded for these objects). However, only 17 B stars were bright enough to be used for the L_X–L_{BOL} analysis, while 45 single O stars spanning the whole range of bolometric luminosities were available in the previous section. The poor statistics definitely require a confirmation of our results with a larger number of objects (see, e.g., Nazé 2009), notably those of lower luminosity, where significant incompleteness biases can arise.

4. ADDITIONAL CORRELATIONS

We also checked for additional correlations besides how L_X–L_{BOL} varies with different stellar subgroups. We remind the reader once again that the X-ray luminosities quoted here are corrected only for the interstellar absorbing column, that the hard X-ray fluxes are unreliable due to the small count rates at such high energies for most of our X-ray sources, and that only few B stars had enough counts to be analyzed spectroscopically.

4.1. $\log(L_X/L_{BOL})$ *versus* L_{BOL}

First, we investigated the $\log(L_X/L_{BOL})$ dependence on the bolometric luminosity (Figure 4). For O stars, there is essentially no trend; the $\log(L_X/L_{BOL})$ relation is thus well constrained to a constant, as seen in the previous section.

One can also look at the evolution of the dispersion around that constant, in the case of single objects but excluding the well-known problematic cases of HD 93250 and Tr16 MJ 496. The dispersions for early-type (O2–O5.5), mid-type (O6–O8), and late-type (O8.5–O9.7) stars were compared using *F*-tests. While early- and mid-type stars display very similar dispersions, that of the late-type stars appears significantly different (at the 1% level), but only in the medium energy band. It could be interpreted as a hint that the weaker stellar winds of late-type stars could be more affected by magnetic confinement than those of early- and mid-type stars;[15] harder, additional X-rays could then contribute to the total high-energy emission when the magnetic field is sufficiently strong, leading to a larger scatter in the medium energy band. Since the stellar winds of hot stars are well known to be radiation-driven, looking at the dispersions as a function of bolometric luminosity should confirm the above trend (i.e., lower luminosity objects should display a larger dispersion in their $\log(L_X/L_{BOL})$). This is not the case, however, as the difference totally disappears: using two luminosity bins, quasi-identical results are found for stars with $\log(L_{BOL})$ above and below 38.5; using three luminosity bins, the largest dispersion is only detected for the total band and the brightest stars ($\log[L_{BOL}] > 38.75$). With such contradictory results, we cannot claim to detect a larger impact of the magnetic confinement on the late-O stars of lower luminosity. This correlates well with the findings by polarimetric surveys of only a few O stars with strong magnetic fields, hence few objects with winds affected by magnetic confinements (see, e.g., Güdel & Nazé 2009, and references therein).

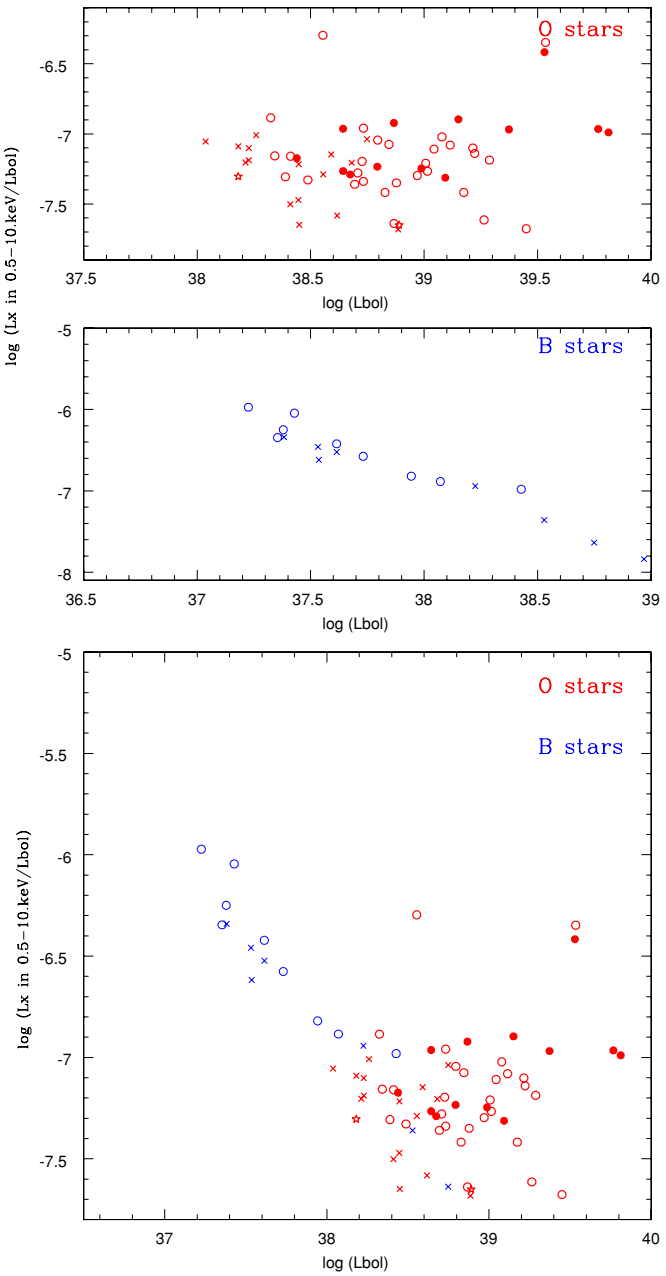

Figure 4. $\log(L_X/L_{BOL})$ as a function of bolometric luminosity for the O (bold red) and B (blue) stars from our sample. Singles and binaries in two strata of detected counts are distinguished using the same symbols as in Figure 3.
(A color version of this figure is available in the online journal.)

For the B stars detected with more than 50 counts, a tight relationship is seen between $\log(L_X/L_{BOL})$ and the bolometric luminosity, especially in the total and medium energy bands (Figure 4). Correlation coefficients in those energy bands reach at least −0.91, and the linear fits yield slopes compatible with minus unity. This may simply reflect the fact that the X-ray luminosity of these B stars appears rather constant with respect to the bolometric luminosity, as already noted in the previous section. The average (log) X-ray luminosities (and their associated dispersions) are 31.16 ± 0.13 in the total band and 30.68 ± 0.20 in the medium band considering all single stars and 31.21 ± 0.14 and 30.78 ± 0.17, respectively, considering

[15] Using the stellar properties of Martins et al. (2005) for O5.5, O7, and O9.5 main-sequence stars, a mass-loss rate derived from these parameters using the recipe of Vink et al. (2000), and a terminal velocity of 2000 km s^{-1}, the magnetic confinement parameter η (ud-Doula & Owocki 2002) reaches the critical unity value for magnetic fields that are 35 G for late-O stars and four times larger, 150 G, for early-type stars: it is thus easier to confine the wind from late-type stars. Similar conclusions are reached when comparing O9.5 supergiants, giants, and main-sequence objects; the magnetic field requirements in this case are 35 G for the latter and 60 G for the former. Note that we did not attempt a refined test, splitting stars into groups of similar spectral types *and* luminosity classes since the O stars in Carina are too few in number to provide a meaningful result in that case.

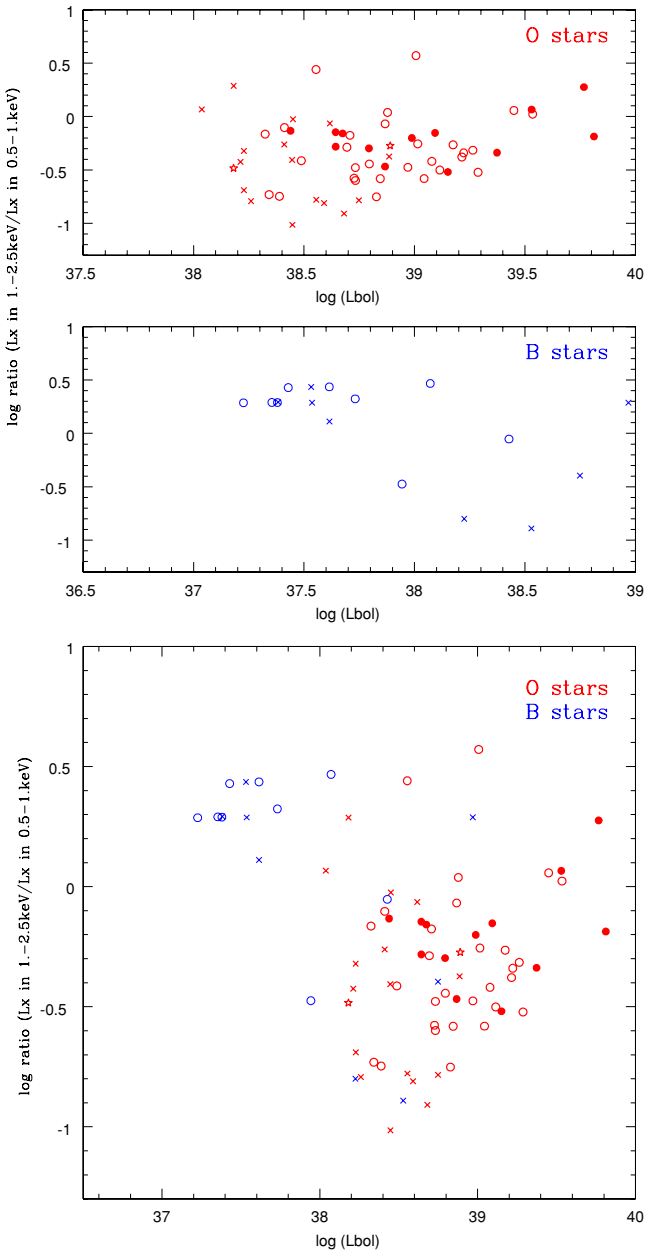

Figure 5. Ratio of the medium and soft X-ray luminosities as a function of the bolometric luminosity for the O (bold red) and B (blue) stars from our sample. Singles and binaries in two strata of detected counts are distinguished using the same symbols as in Figure 3.

(A color version of this figure is available in the online journal.)

only the single B stars with >100 counts. We caution however that such luminosities are close to the brightness limit for spectral analysis (the average detection limit is $\sim 10^{30}$ erg s^{-1}, and 50 counts are needed for a rough spectral analysis). Clearly, a more extensive and sensitive study is needed to confirm the nearly constant luminosity of these B stars (see also Section 7 below).

As mentioned in the introduction, the X-ray emission of B stars, since it is observed only for a small fraction of objects, may not be linked to the B-star itself but to a close PMS object, either a physical companion or a line-of-sight coincidence in dense clusters (see also Evans et al. 2011, for more on this subject). Indeed, when flaring, such PMS stars often reach 10^{30} erg s^{-1} and even in some rare cases 10^{31} erg s^{-1} (Güdel & Nazé 2009). The observed luminosity of the X-ray-brightest B stars in Carina is thus compatible with the maximum luminosity of flaring PMS stars. Since such luminosities are only reached during flares, we should detect a strong variability of our sources if their X-ray emission is due to PMS flaring, but the lack of counts prevents us from deriving light curves for all objects. Also we do not see any clear connection between a high X-ray luminosity and flares even when flares are detected (for more details, see Gagné et al. 2011 and Evans et al. 2011). In addition, the hard spectra of B stars appear compatible with the PMS scenario but in some peculiar B stars, magnetic phenomena can also produce hard X-ray emission (see the case of σ Ori E Sanz-Forcada et al. 2004; ud-Doula et al. 2006). Finally, it should be noted that a gradual transition of behaviors is observed between late-O stars and the brightest, earliest B stars (see below). This could therefore advocate for an intrinsic source of X-rays in (at least some) early B stars, such as embedded-wind shocks for the earliest ones and magnetically confined winds for some others.

4.2. Hardness Ratios

A second analysis involved the hardness ratio, defined as the ratio of the medium to soft (unabsorbed) X-ray luminosities (Figure 5). In the B stars, this ratio appears at 0.3–0.4 dex for most objects; it corresponds to the ratio of a plasma with a temperature of $\gtrsim$1.5 keV in the absence of absorption. This value is clearly above the average ratio for O stars, but it should be noted that the brightest objects have a lower ratio which is quasi-identical to that of late-O stars. Looking at this ratio as a function of spectral type or luminosity class confirms the trend. The earliest B stars (B0) display low hardness ratios (i.e., the X-ray emission is soft) compared to their slightly later (B1–B2) counterparts; a similar trend is seen when comparing supergiant B stars with their main-sequence counterparts. Note however that the number of B stars bright enough to yield a usable spectrum in the CCCP is low, and that this may blur the trends—indeed, the three supergiant B stars are all of type B0.

Concerning O stars, there appears to be no trend with luminosity class, and the relation with spectral type appears scattered (the only conclusion being that low ratios are not favored in the case of the earliest O stars). However, an overall shallow trend appears when hardness ratio is plotted versus the bolometric luminosity. Indeed, except for a few faint stars (for which the 1.0–2.5 keV fluxes are uncertain, see crosses in Figure 5) and the peculiar Tr16 MJ 496, harder X-ray emission seems to correlate loosely with higher bolometric luminosities. However, the correlation coefficient is far from being significant due to the large scatter. In the framework of the wind-shock model, there may be two possible causes for this shallow trend. First, this could be an absorption effect. The brightest stars have stronger, hence more dense, stellar winds, which can lead to a larger intrinsic absorption and therefore a harder appearance of the spectrum. Our fits provide estimates of the circumstellar absorption, but its correlation with hardness ratio again seems quite shallow and scattered, thus not formally significant (Figure 6), and as already mentioned in Section 2.1, there is no trend whatsoever between this additional column and the bolometric luminosity. Second, Walborn et al. (2009) detected (1) a larger ionization of the plasma in early-type stars (implying a hotter plasma) and (2) a shift of the overall spectral distribution toward lower energies for late-type stars. These trends, if confirmed, would also be compatible with a higher hardness ratio toward larger bolometric luminosities. Without detailed hydrodynamic simulations and better statistics, it is still

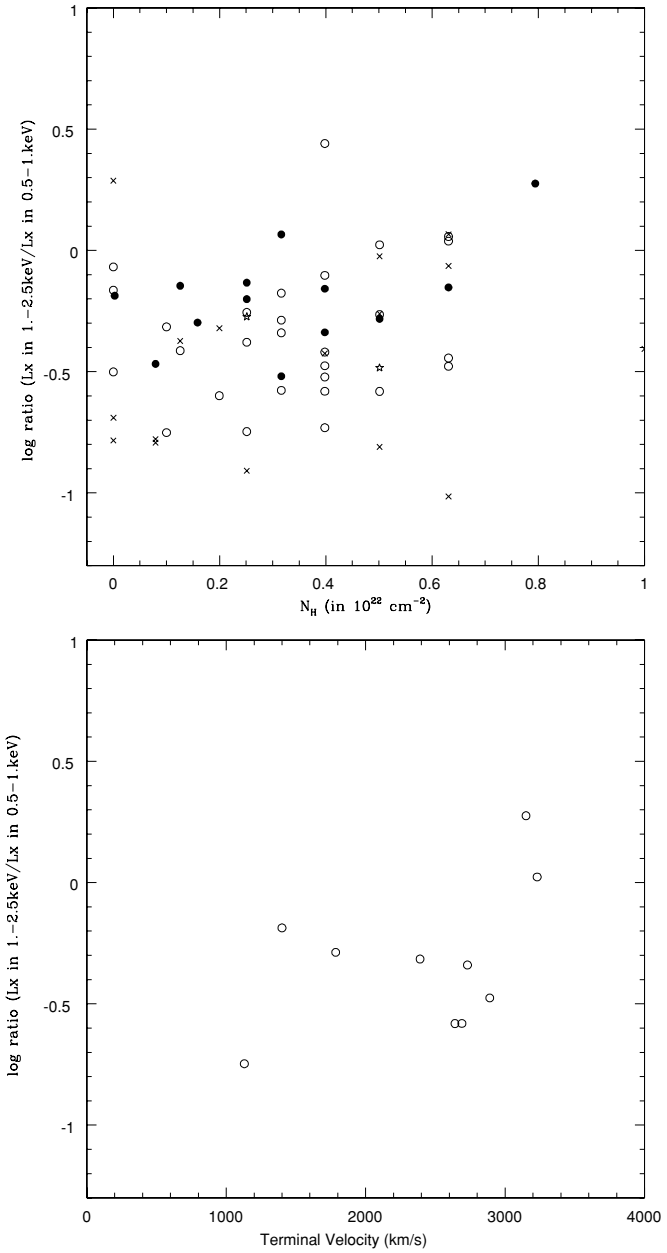

Figure 6. Ratio of the medium and soft X-ray luminosities for O stars as a function of the additional absorbing column (top) and terminal wind velocity (when available, bottom). Symbols are the same as in Figure 3.

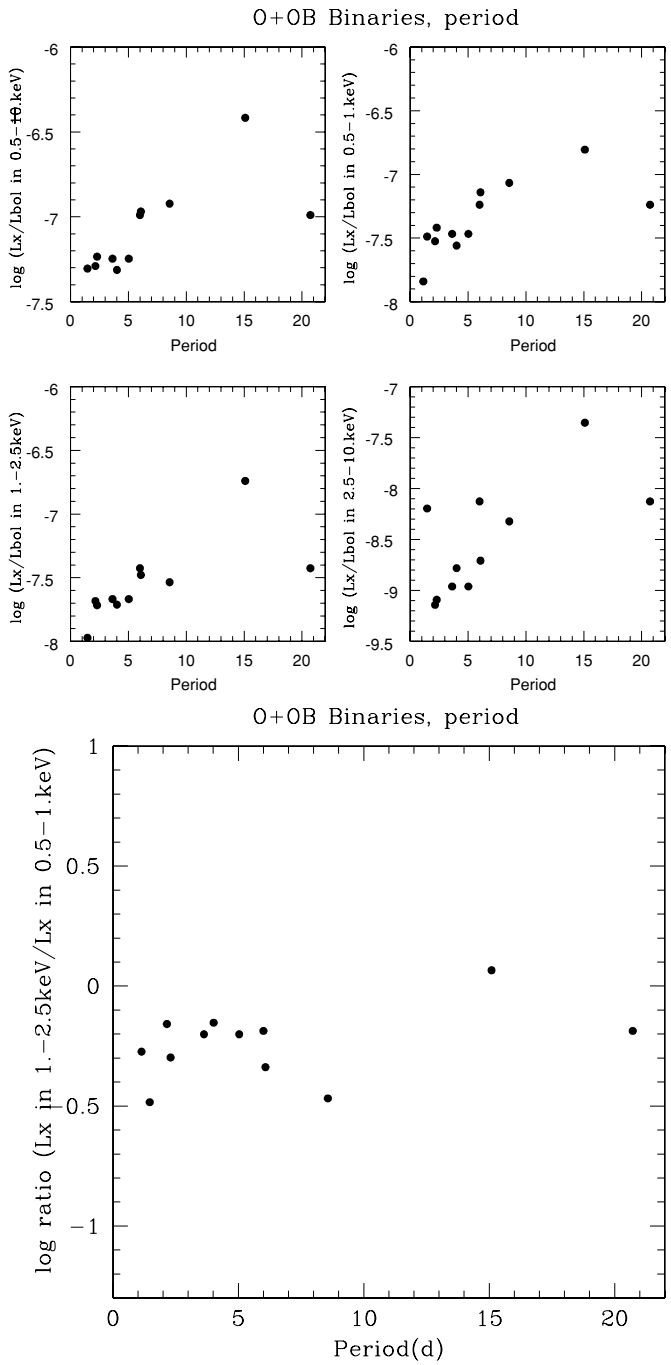

Figure 7. $\log(L_X/L_{BOL})$ and hardness ratio as a function of the period (in days) for O+OB binaries. Note that a given object can appear twice if it is actually composed of two binary systems (e.g., QZ Car).

unclear whether the hotter plasma, the higher absorption, or a combination of both effects is the cause of this shallow trend.

Finally, as the X-ray emission from hot stars originates from their stellar winds, correlations of the hardness ratios with wind parameters should be investigated. As reliable, homogeneous mass-loss rates are unavailable for our sample stars, we used only the terminal wind speeds from Howarth et al. (1997). Ten O-type stars are in common between Howarth's catalog and this survey. Again, a shallow trend (in the sense of harder emission for faster winds; see Figure 6) may be present but the scatter is large and the trend detected by eye is clearly dominated by the two extreme stars, HD 93027 (low v_∞, low hardness ratio) and HD 93129A (high v_∞, high hardness ratio), casting doubt on its existence.

In any case, what seems obvious from the different tested relationships is that the brightest and earliest B stars behave like the faintest and latest O stars and that there is a gradual transition toward B stars of later types (B1–B2). This continuum of behaviors could be explained by wind-shock emission essentially vanishing below bolometric luminosities of about 10^{38} erg s^{-1}, where another mechanism of X-ray production, probably magnetic in nature, dominates.

5. BINARIES

We will here discuss only O+OB systems since no B+B binary had enough counts for a spectral study.

As can be seen from Table 4 and Figure 3, the L_X–L_{BOL} ratios of O+OB binaries appear quite similar to those of single O stars,

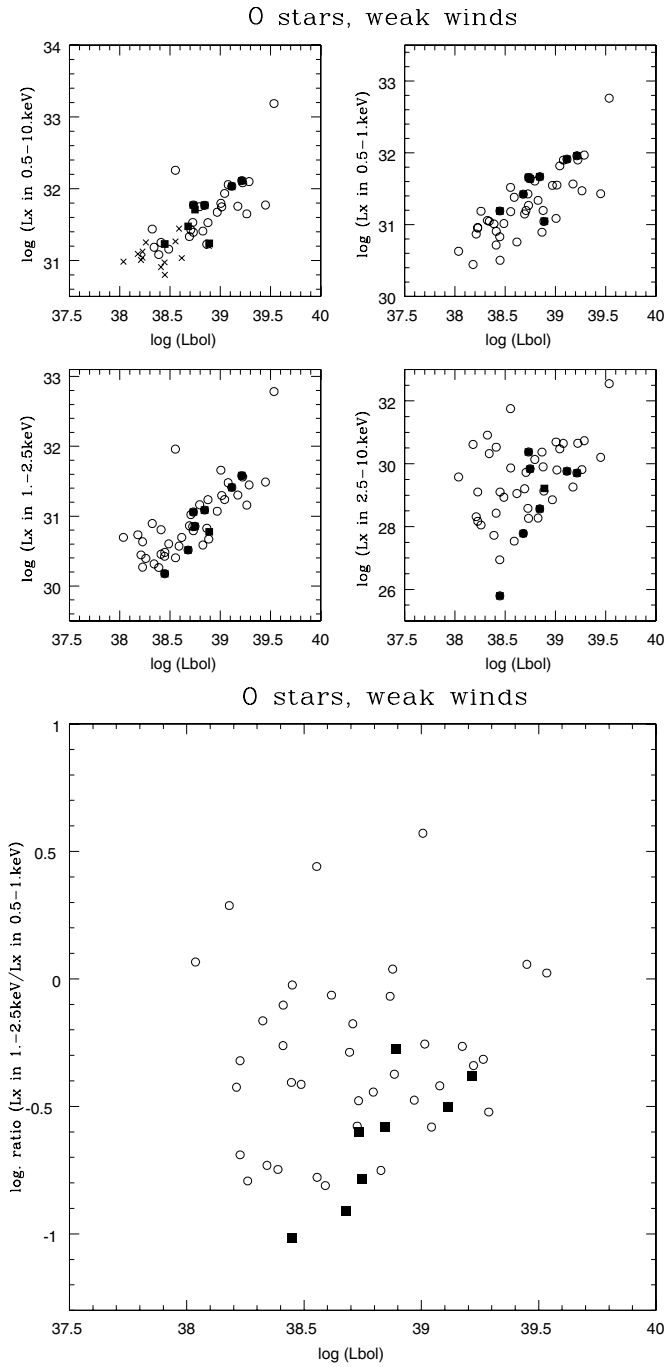

Figure 8. Total X-ray luminosity (top) and ratio of the medium-to-soft fluxes (bottom) for weak-wind stars (filled squares) and "normal," single O stars (open circles).

with the exception of the bright system HD 93403 (a known colliding-wind binary; see Rauw et al. 2002). This general lack of strong overluminosity was already found in Oskinova (2005), as well as for most binaries of NGC 6231 (Sana et al. 2006), Carina OB1 (Antokhin et al. 2008), and the 2XMM survey (Nazé 2009). It is confirmed here for the known massive binaries in the Carina Nebula. Thus, there appear to be only a few exceptional systems where the collisions are X-ray-bright, the impact of wind–wind collision being small in most systems. Nevertheless, binaries and single objects are not 100% equal. First, their average temperatures ($\langle kT \rangle = \sum kT_i \times \mathrm{norm}_i / \sum \mathrm{norm}_i$) are slightly larger (for 1T fits: 0.47 keV versus 0.55 keV for singles and binaries, respectively, for 2T fits: 0.71 keV versus 0.83 keV for singles and binaries, respectively) but the differences are not significant (at the 1% level), due to the large dispersion in average temperatures (up to 1 keV). Second, it must be noted that, whatever the energy band, the $\log(L_X/L_{BOL})$ values of binaries are systematically larger than those of single stars (as can be seen by looking at rows 4 and 5 versus rows 9 and 10 of Table 4). However, except for the medium energy band (which is hard enough to be potentially affected by some wind–wind emission), the differences are again not formally significant (at the 1% level).

Additional relations were also searched for in O+OB binaries, notably between $\log(L_X/L_{BOL})$ and the binary properties (total bolometric luminosity, eccentricity, period, semi-major axis; see Figure 7). The most obvious trends are larger $\log(L_X/L_{BOL})$ ratios for longer periods, combined bolometric luminosity, or larger separation. However, these trends are clearly dominated by HD 93403, the only known binary in the survey with period $P > 10$ days (the second binary of the QZ Car system has a period of 20 days, but the X-ray emission of QZ Car cannot be related exclusively to that system; see Parkin et al. 2011). Adding the binaries of NGC 6231 (Sana et al. 2006) totally blurs the picture. Indeed, for a large sample, Nazé (2009) found no strong relation (i.e., a very large scatter) between $\log(L_X/L_{BOL})$ and binary periods. Finally, while HD 93403 stands out with its slightly harder emission and rather long period, the hardness ratios of the other O+OB binaries do not seem to correlate with their periods.

The small impact of wind–wind emission in the X-ray range can be qualitatively explained by two reasons. First, the winds collide at low speed in close binaries whereas the collision in wide systems is adiabatic, hence emitting few photons; there is thus a small region of parameter space where the conditions are just right for getting an X-ray-bright wind–wind collision—this would be the case for HD 93403. Second, it now seems difficult to get ram pressure balance in many systems where the wind momenta of the components are very different; in most cases, modeling shows that the stronger wind crashes onto its companion (Pittard & Parkin 2010). To test these ideas quantitatively, comparisons of similar stellar pairs with, e.g., different periods are needed. However, although the Carina Nebula contains many objects, there are not enough cases of binaries to perform such a study.

6. WEAK-WIND OBJECTS

The weak-wind problem in hot stars is twofold. On the one hand, some weak-wind stars have lower mass-loss rates than other stars of similar spectral type; on the other hand, other weak-wind stars have lower mass-loss rates than what atmospheric models predict. To explain the weakness of the winds, high X-ray luminosities have sometimes been invoked as they can modify the wind ionization, hence the efficiency of the wind acceleration (Martins et al. 2005; Marcolino et al. 2009).

In our survey, six stars of the peculiar Vz type (Walborn 2009) have been detected: HD 93128, HD 93129B, CPD –58°2611, CPD –58°2620, HD 303311, and FO 15. Adding HD 93028 and possibly HD 93146 from Martins et al. (2005), this makes eight stars with potential "weak-wind" problems. In our data set, these eight objects display normal total X-ray luminosities. A similar conclusion was found for HD 46202, the only other weak-wind object which has been recently re-observed in X-rays: while old *Einstein* data seemed to imply a large $\log(L_X/L_{BOL}) =$

Table 5
Properties of X-ray Sources with <50 counts

CXOGNC J	Name	Sp. Type	Bin?	$\log(L_{BOL}/L_{\odot})$	Net Counts (counts)	Ph. Flux (photons cm^{-2} s^{-1})	Med. En.	$\log(L_X)$	$\log(L_X/L_{BOL})$
104039.26−600536.1	LS 1745	B2 III		3.76	$16.0^{22.5}_{10.1}$	2.08e-6	1.12	30.59	−6.75
104112.33−595825.0	HD 92741	B1.5 II:		4.98	$23.8^{29.6}_{18.6}$	1.82e-6	1.01	30.53	−8.03
104135.44−593945.6	HD 303225	B1.5 V		4.02	$13.1^{17.2}_{9.7}$	9.84e-7	1.07	30.27	−7.34
104213.35−590946.2	HD 303297	B1 V		4.23	$38.3^{45.4}_{31.7}$	3.47e-6	1.03	30.82	−7.00
104225.08−590924.7	HD 303296	B1 Ve		4.24	$15.5^{20.4}_{11.3}$	1.26e-6	1.00	30.38	−7.45
104236.31−595926.0	CPD-59 2495	B1.5 V		3.71	$15.4^{20.4}_{11.1}$	1.21e-6	1.42	30.36	−6.93
104245.15−595219.5	HD 305437	B0.5 V		4.50	$28.3^{34.6}_{22.6}$	3.07e-6	0.85	30.76	−7.32
104303.96−595139.0	HD 305515	B1.5 Vsn:		3.77	$8.6^{12.7}_{5.1}$	8.02e-7	1.34	30.18	−7.17
104315.77−595105.9	HD 305516	B0.5 V		4.33	$26.3^{33.0}_{20.2}$	2.33e-6	1.18	30.64	−7.28
104316.35−591027.2	HD 93026	B1.5 V		4.09	$8.8^{12.2}_{6.1}$	6.32e-7	1.22	30.08	−7.60
104330.86−592923.8	HD 303312	B0 V(n)		4.71	$3.7^{43.2}_{30.8}$	3.21e-6	0.97	30.78	−7.51
104333.41−593511.1	Cl* Trumpler 14 MJ 71	B1 Ia		4.81	$9.1^{12.6}_{6.2}$	7.32e-7	1.31	30.14	−8.25
104348.82−593335.2	Cl* Trumpler 14 MJ 128	B2 V		3.54	$28.6^{34.3}_{23.5}$	2.16e-6	1.57	30.61	−6.51
104355.20−593314.7	Cl* Trumpler 14 MJ 163	B0 V		4.35	$23.1^{28.4}_{18.5}$	1.72e-6	1.29	30.51	−7.42
104355.21−593239.3	Cl* Trumpler 14 MJ 161	B2 V		3.30	$5.4^{8.3}_{3.3}$	1.35e-6	0.97	30.41	−6.47
104357.57−593338.6	Cl* Trumpler 14 MJ 178	B1 V		4.05	$16.5^{21.0}_{12.7}$	1.25e-6	1.29	30.37	−7.26
104359.45−600513.3	CPD-59 2555B	O9.5 V		4.44	$6.4^{9.4}_{4.0}$	1.43e-6	0.90	30.56	−7.46
104359.55−593231.7	Cl* Trumpler 14 MJ 189	B1 V		4.25	$4.3^{7.0}_{2.4}$	3.25e-7	1.16	29.79	−8.05
104359.86−593524.1	Cl* Trumpler 16 MJ 195	B1 V		4.44	$45.3^{53.0}_{37.7}$	2.25e-6	1.42	30.63	−7.40
104400.43−600559.8	CPD-59 2554	O9 V		4.83	$35.9^{42.4}_{29.5}$	7.11e-6	0.88	31.26	−7.15
104400.94−593545.7	Cl* Trumpler 14 MJ 200	O9 V		4.74	$33.2^{39.4}_{27.6}$	2.60e-6	0.99	30.82	−7.50
104402.44−592936.3	Cl* Trumpler 14 MJ 203	O9 III		4.52	$45.0^{52.4}_{37.6}$	4.92e-6	1.04	31.10	−7.00
104405.86−595941.5	HD 305520	B1 Ib		5.01	$40.8^{47.5}_{34.6}$	3.05e-6	1.12	30.76	−7.84
104414.93−600005.5	HD 305522	B0.5 V		4.44	$3.5^{5.9}_{1.8}$	2.86e-7	0.99	29.73	−8.29
104432.90−594026.1	Cl* Trumpler 16 MJ 339	B1 V		4.01	$7.6^{11.7}_{4.1}$	3.44e-7	1.14	29.81	−7.78
104435.12−592328.1	Cl Trumpler 15 20	O9 V:		3.70	$2.7^{4.9}_{1.3}$	2.52e-7	1.44	29.81	−7.47
104435.91−592335.7	Cl Trumpler 15 19	O9 V		3.70	$9.6^{13.3}_{6.2}$	1.24e-6	2.17	30.50	−6.78
104436.89−600111.6	CPD-59 2593	B0.5 V + B0.5 V	Y	4.26	$22.1^{27.5}_{17.3}$	1.78e-6	1.38	30.52	−7.32
104437.15−594001.5	Cl* Trumpler 16 MJ 357	B0.5 V		4.14	$6.1^{9.7}_{3.2}$	3.10e-7	1.77	29.77	−7.96
104437.69−592307.2	Cl Trumpler 15 21	B0 III		3.45	$2.8^{4.9}_{1.3}$	2.66e-7	1.31	29.70	−7.33
104441.00−594009.9	Cl* Trumpler 16 MJ 372	B0 V		4.38	$14.2^{19.8}_{9.2}$	5.78e-7	0.93	30.04	−7.93
104442.35−592304.0	CPD-58 2656	B0.5 IV-V		4.33	$13.9^{18.0}_{10.5}$	8.69e-6	1.04	31.21	−6.70
104443.77−592117.2	CPD-58 2659B	O9.5 III:		4.67	$16.7^{21.2}_{12.9}$	1.28e-6	0.96	30.52	−7.74
104446.54−592154.0	CPD-58 2662	B2 V		3.49	$6.7^{9.8}_{4.4}$	5.13e-7	1.41	29.99	−7.09
104447.51−595759.0	HD 305534	B0.5 V: + B1 V:	Y	4.52	$22.0^{29.6}_{14.5}$	9.00e-7	1.51	30.23	−7.87
104450.39−595545.0	Cl* Trumpler 14 MJ 420	B1 V		3.96	$42.9^{53.0}_{32.8}$	1.63e-6	1.01	30.49	−7.05
104453.76−593748.3	Cl* Trumpler 16 MJ 424	B2 V		3.86	$10.2^{15.2}_{5.8}$	5.61e-7	1.35	30.02	−7.41
104457.33−600046.7	LS 1866	B2 V		3.94	$6.9^{10.6}_{3.9}$	7.02e-7	2.45	30.12	−7.40
104459.90−594314.8	CPD-59 2618	B1.5 V		3.80	$9.5^{13.0}_{6.6}$	2.72e-6	1.12	30.71	−6.67
104503.20−594012.1	Cl* Trumpler 16 MJ 467	B0.5 V		4.03	$6.6^{10.7}_{3.1}$	3.27e-7	1.69	29.79	−7.82
104509.65−594008.5	Cl* Trumpler 16 MJ 499	B2 V		3.32	$3.4^{6.6}_{0.8}$	1.81e-7	0.90	29.53	−7.37
104512.62−594248.4	Cl* Trumpler 16 MJ 513	B2 V		4.04	$14.9^{19.4}_{11.1}$	7.35e-7	1.76	30.14	−7.48
104513.44−595753.1	HD 305533	B0.5 Vnn_shell:		4.48	$24.4^{30.8}_{18.5}$	3.95e-6	1.42	30.87	−7.19
104517.57−592337.4	HD 93342	B1 Iab-Ib		5.45	$4.7^{7.5}_{2.5}$	4.02e-7	1.64	29.88	−9.16
104546.52−600513.5	HD 305538	B0 V		4.23	$32.5^{39.5}_{26.0}$	2.64e-6	1.35	30.70	−7.12
104553.45−600537.0	CPD-59 2660	B0.5 V		4.10	$4.8^{7.6}_{2.6}$	9.19e-7	1.48	30.24	−7.45
104715.29−600538.8	Cl Bochum 11 5	O9 V?		4.78	$43.7^{50.7}_{37.3}$	3.22e-6	0.94	30.92	−7.45
104801.65−593903.1	HD 93723	B3 III		4.18	$27.0^{37.9}_{16.1}$	1.20e-6	1.64	30.35	−7.41
104855.29−592649.3	HD 93873	B1 Ia		5.60	$15.1^{20.5}_{10.2}$	1.22e-6	1.20	30.36	−8.82
104858.98−594109.0	HD 303413	B1 Ib		4.40	$17.1^{21.7}_{13.1}$	1.28e-6	1.07	30.38	−7.60
104925.87−600137.3	HD 305606	B2 V		3.57	$7.6^{11.9}_{3.8}$	8.00e-7	0.96	30.18	−6.97

Note. The X-ray luminosities have been corrected for the interstellar absorption only (see the text).

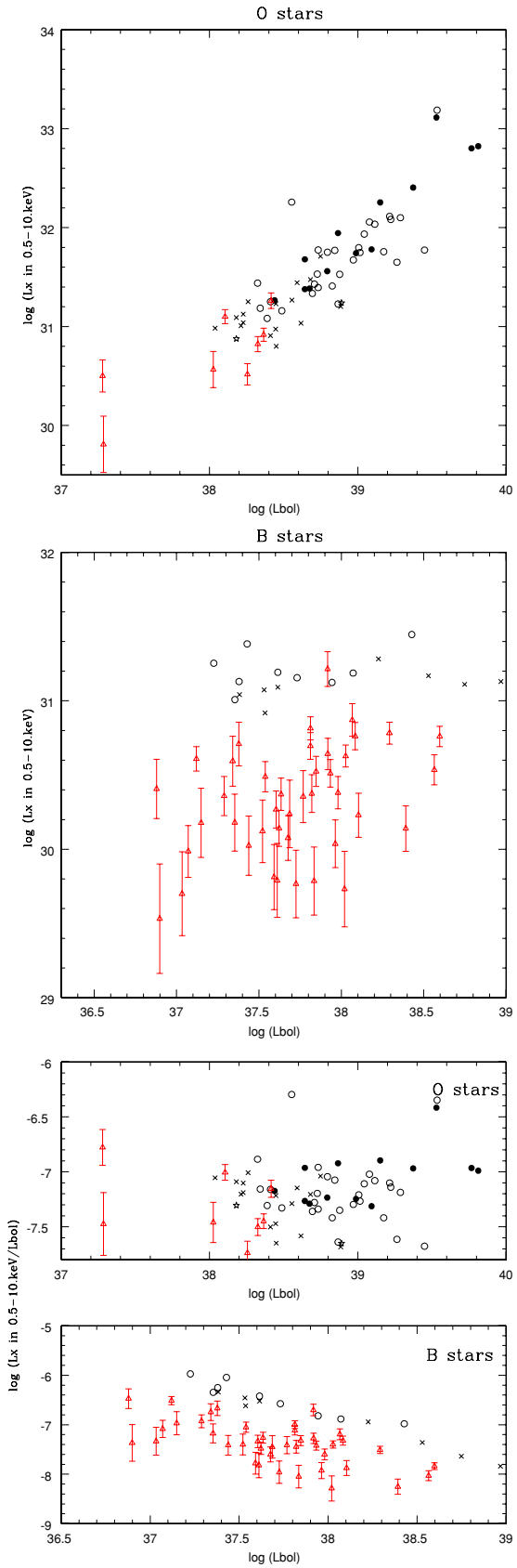

Figure 9. X-ray luminosity and $\log(L_X/L_{BOL})$ as a function of the bolometric luminosity, for O stars and B stars. Singles and binaries in two strata of detected counts are distinguished using the same symbols as in Figure 3. Faintest objects (<50 counts) in a third stratum of detected counts are shown by (red) triangles with error bars.

(A color version of this figure is available in the online journal.)

−6, with a large impact on the ionization structure hence the wind propulsion (Martins et al. 2005), *Chandra* observations show the star to have $\log(L_X/L_{BOL}) = -7$ (Wang et al. 2008). Such "canonical" X-ray luminosities are probably insufficient to induce some wind-decreasing effect ($\log(L_X/L_{BOL}) = -3.5$ might be necessary, see Marcolino et al. 2009). It is however interesting to note that the $\log(L_X/L_{BOL})$ values in the soft and medium bands generally differ by 0.2–0.4 dex (see Table 4; only the supergiant O stars have a smaller difference but the sample size is just two objects), while this difference amounts to 0.6 dex in these eight stars. The X-ray emission of these potential "weak-wind" stars thus appears softer than the other stars of our sample although this is not a significant result (at the 1% level; Figure 8).

7. THE FAINTEST DETECTED O AND B STARS

With at most 50 counts, the faintest O and B stars (eight O stars, 41 single B stars, and two B+B binaries) detected in this survey could not be analyzed spectroscopically on an individual basis. Stacking the data yields a composite spectrum for the single O stars detected with <50 counts and a separate composite spectrum for the single B stars detected with <50 counts. Stacked spectra are always dominated by the strongest of the X-ray sources that were stacked, but we note that only about 10% of these faint OB stars have substantially fewer counts than the others of the same category, limiting the consequences of stacking. These combined spectra were fitted by models similar to those described in Section 2 for individual stars, using an average interstellar column of 2.6×10^{21} cm^{-2} for the O stars and 2.2×10^{21} cm^{-2} for the B stars (which corresponds to the average interstellar column for these two stellar groups). The parameters of the fits can be found at the bottom of Table 2. These fits permit to find the conversion factor between photon fluxes and (unabsorbed) energy fluxes in the total band (the most reliable since it has the maximum number of counts): a unit photon flux corresponds to absorption-corrected energy fluxes of 4.05×10^{-9} erg cm^{-2} s^{-1} for O stars and 2.98×10^{-9} erg cm^{-2} s^{-1} for B stars. We then assume that the spectral parameters obtained from fitting the composite spectrum can be applied to each faint source individually. Table 5 provides the X-ray source name and the stellar identification (Columns 1 and 2), the spectral type (Column 3), the binary status (Column 4), the bolometric luminosity (Column 5), the number of net counts in the 0.5–8.0 keV band together with their associated 68% confidence interval (Column 6), the photon flux (Column 7), the median energy of the recorded counts (Column 8), the absorption-corrected X-ray luminosity in the total energy band (Column 9), and the L_X–L_{BOL} ratio in the same energy band (Column 10). Columns 6–8 are reproduced from the CCCP catalog (Broos et al. 2011), and Columns 2–5 from the stellar catalog (Povich et al. 2011; Gagné et al. 2011). Figure 9 graphically illustrates the results. Error bars were estimated using the relative errors on the net counts; they are shown for demonstration purposes only (they are no perfect estimates of the actual errors since they do not take into account the modeling errors).

For O stars, the eight faint objects, all of late spectral type, clearly follow the L_X–L_{BOL} relation traced by the brighter stars, confirming the above results. For B stars, however, the 41 faint stars do not behave as the other objects although all are of early-B spectral types (B0–B2). With similar bolometric luminosities but much lower X-ray luminosities, the faint objects simply populate the bottom part of the graphics. Although $\log(L_X/L_{BOL})$ still decreases with bolometric luminosity, it is

Table 6
Properties of the Undetected OB Stars

R.A. (hh mm ss)	Decl. (dd mm ss)	Name	Sp. Type	Bin?	$\log(L_{BOL}/L_{\odot})$	Upper Limit on Net Counts (counts)	Upper Limit on Photon Flux (photons cm^{-2} s^{-1})	Upper Limit on $\log(L_X)$	Upper Limit on $\log(L_X/L_{BOL})$
10 40 30.10	−59 56 51.3	HD 305443	B2 III		3.71	5.7	5.46e-7	30.01	−7.28
10 41 15.31	−59 57 45.5	LS 1760	B2 Ib		4.11	1.5	1.22e-7	29.36	−8.33
10 41 20.28	−60 06 36.4	LS 1763	B2 V		3.54	1.4	1.12e-7	29.32	−7.80
10 41 54.20	−59 06 36.5	HD 92852	B1 V		4.16	7.5	7.16e-7	30.13	−7.62
10 41 55.83	−59 16 16.7	HD 303202	B3 III		3.80	2.8	2.36e-7	29.65	−7.74
10 41 59.21	−59 07 49.8	HD 303189	B2 V		3.70	1.2	2.55e-7	29.68	−7.61
10 42 02.30	−60 08 38.6	HD 305452	B2 III		4.11	2.5	2.04e-7	29.58	−8.11
10 42 07.61	−59 54 24.1	HD 92877	B2 III		4.22	13.3	6.07e-7	30.06	−7.74
10 42 11.69	−59 08 29.4	LS 1778	B1 Vn		3.95	9.2	8.06e-7	30.18	−7.35
10 42 15.83	−59 08 13.9	HD 92894	B0 IV		4.62	3.8	4.28e-7	29.91	−8.30
10 42 32.17	−59 35 30.4	HD 92937	B2.5 II:		4.24	2.8	2.53e-7	29.68	−8.14
10 42 40.57	−59 12 56.6	HD 92964	B2.5 Ia		5.87	1.1	1.17e-7	29.34	−10.11
10 42 44.06	−59 07 07.4	LS 1790	B0.5 IV/Vne		3.89	2.5	2.05e-7	29.59	−7.88
10 42 50.17	−59 25 31.2	HD 303313	B1.5 V		3.98	1.1	9.59e-8	29.26	−8.30
10 42 54.63	−59 58 19.6	HD 305535	B2.5 Vn		3.91	7.1	3.22e-7	29.78	−7.71
10 43 01.54	−59 20 23.7	HD 303299	B1 Ve		4.66	1.1	9.08e-8	29.23	−9.01
10 43 04.14	−59 04 59.7	HD 93002	B0 IV/V		4.43	1.1	9.14e-8	29.24	−8.78
10 43 10.09	−60 02 11.7	HD 305543	B1 III		4.04	2.6	2.25e-7	29.63	−7.99
10 43 27.40	−60 05 54.7	HD 93056	B1 V		4.43	6.3	5.76e-7	30.04	−7.98
10 43 43.89	−59 33 46.1	Cl* Trumpler 14 MJ 102	O9 V		4.42	3.3	2.79e-7	29.86	−8.15
10 43 46.98	−60 05 49.2	HD 93097	B0 Vn		4.32	5.3	5.18e-7	29.99	−7.91
10 43 48.87	−60 09 00.7	CPD-59 2543	B1.5 V		3.49	7.4	7.05e-7	30.12	−6.95
10 43 49.40	−59 57 22.6	HD 305521	B0.5 Vn		4.40	3.7	1.27e-6	30.38	−7.60
10 43 50.90	−59 33 50.5	Cl* Trumpler 14 MJ 136	B1 V		3.93	2.3	1.88e-6	30.55	−6.97
10 43 53.65	−59 33 00.6	Cl* Trumpler 14 MJ 149	B0.5 IV-V+B	*Y*	4.38	1.1	6.86e-7	30.11	−7.85
10 43 56.03	−59 34 41.0	Cl* Trumpler 14 MJ 170	B2 V		3.71	1.1	9.34e-8	29.25	−8.04
10 43 58.00	−59 32 30.6	Cl* Trumpler 14 MJ 180	B2 V		3.16	1.1	9.08e-8	29.23	−7.51
10 43 59.88	−59 31 47.1	Cl* Trumpler 14 MJ 191	B7 V		2.91	2.2	2.36e-7	29.65	−6.85
10 44 00.62	−59 25 49.2	LS 1822	B1.5 Ib		4.11	12.6	5.90e-7	30.05	−7.65
10 44 13.80	−59 42 57.1	Cl* Trumpler 16 MJ 261	B0 V		4.57	6.9	3.67e-7	29.84	−8.31
10 44 14.74	−59 42 51.7	Cl* Trumpler 16 MJ 263	B0.5 V		4.33	5.1	2.71e-7	29.71	−8.20
10 44 15.87	−60 09 04.1	LS 1837	B1 V		3.88	...	...	...	...
10 44 24.62	−59 30 35.8	Cl* Trumpler 14 MJ 291	B1 V?		3.98	1.8	1.61e-7	29.48	−8.08
10 44 25.49	−59 33 09.2	Cl* Trumpler 14 MJ 299	B1.5 V		3.74	1.1	8.93e-8	29.23	−8.10
10 44 26.47	−59 41 02.8	Cl* Trumpler 16 MJ 306	B1.5 V		4.14	4.1	1.44e-7	29.43	−8.29
10 44 28.97	−59 42 34.3	Cl* Trumpler 16 MJ 323	B2 V		3.31	3.1	1.58e-7	29.47	−7.42
10 44 29.10	−59 20 05.0	LS 1842	B1 V		3.94	1.1	9.19e-8	29.24	−8.29

Table 6
(Continued)

R.A. (hh mm ss)	Decl. (dd mm ss)	Name	Sp. Type	Bin?	$\log(L_{BOL}/L_{\odot})$	Upper Limit on Net Counts (counts)	Upper Limit on Photon Flux (photons cm^{-2} s^{-1})	Upper Limit on $\log(L_X)$	Upper Limit on $\log(L_X/L_{BOL})$
10 44 29.42	−59 38 38.1	Cl* Trumpler 16 MJ 321	B1 V		3.98	5.2	4.80e-7	29.96	−7.61
10 44 30.48	−59 41 40.5	Cl* Trumpler 16 MJ 329	B1 V		4.05	3.4	1.41e-7	29.42	−8.21
10 44 30.77	−59 21 26.0	CPD-58 2647	B0 V		4.07	1.1	1.59e-7	29.48	−8.18
10 44 32.66	−59 20 38.5	Cl Trumpler 15 25	B5 V		2.59	3.7	2.93e-7	29.74	−6.43
10 44 36.35	−59 24 20.3	Cl Trumpler 15 18	O9 I/II:(e:)		5.61	1.1	9.67e-8	29.39	−9.80
10 44 36.76	−59 54 24.9	Cl* Trumpler 14 MJ 366	B1 Ib		5.50	6.3	6.16e-7	30.06	−9.02
10 44 38.64	−59 48 14.1	Cl* Trumpler 16 MJ 369	B1 V		4.06	1.6	9.00e-8	29.23	−8.41
10 44 40.31	−59 41 48.9	Cl* Trumpler 16 MJ 370	B1 V		4.19	1.8	9.21e-8	29.24	−8.54
10 44 40.58	−59 21 13.7	Cl Trumpler 15 4	B1 Vn		3.88	1.1	2.20e-7	29.62	−7.85
10 44 40.68	−59 22 28.6	CPD-58 2653	B2.5 IV-V		3.77	2.4	8.67e-7	30.21	−7.14
10 44 42.12	−59 22 30.5	Cl Trumpler 15 13	B1 V		4.02	1.1	5.42e-7	30.01	−7.60
10 44 42.35	−59 22 02.9	Cl Trumpler 15 9	B1 V		3.46	2.3	3.19e-7	29.78	−7.26
10 44 42.76	−59 21 51.0	CPD-58 2657	B2.5 Vn		3.78	1.1	9.31e-8	29.24	−8.12
10 44 44.48	−59 21 32.8	CPD-58 2659C	B2 Vn		3.81	1.1	9.26e-8	29.24	−8.15
10 44 49.87	−59 24 46.9	Cl Trumpler 15 17	B5 V		2.64	1.1	9.81e-8	29.27	−6.96
10 44 56.28	−59 33 03.5	Cl* Trumpler 16 MJ 434	B0.5 V	*Y*	4.33	1.8	1.73e-7	29.51	−8.40
10 45 00.24	−59 43 34.4	CPD-59 2616	B2 V		3.66	2.7	1.52e-7	29.46	−7.79
10 45 02.15	−59 42 01.0	Cl* Trumpler 16 MJ 466	B1 V		3.99	4.4	2.26e-7	29.63	−7.94
10 45 05.19	−59 41 42.3	Cl* Trumpler 16 MJ 477	B1 V		3.73	3.9	2.01e-7	29.58	−7.73
10 45 05.87	−59 44 18.8	Cl* Trumpler 16 MJ 483	B2 V		3.56	5.0	2.54e-7	29.68	−7.47
10 45 09.74	−59 42 57.2	Cl* Trumpler 16 MJ 501	B1 V		3.86	3.9	4.69e-7	29.95	−7.50
10 45 11.19	−59 41 11.2	Cl* Trumpler 16 MJ 506	B1 V		3.99	4.2	2.16e-7	29.61	−7.97
10 45 16.72	−59 54 45.7	HD 305528	B2 V		3.81	1.9	1.58e-7	29.47	−7.92
10 45 19.42	−59 39 37.4	Cl* Trumpler 16 MJ 547	B1.5 V		3.49	2.0	1.21e-7	29.36	−7.71
10 45 22.13	−59 37 38.5	Cl* Trumpler 16 MJ 558	B2 V		3.60	24.8	8.55e-7	30.21	−6.98
10 46 25.42	−60 08 43.7	LS 1893	B0 V		4.09	5.3	3.49e-7	29.82	−7.86
10 47 09.20	−59 47 29.7	HD 93620	B2 II/III		4.28	1.1	8.49e-8	29.20	−8.66
10 47 13.16	−60 13 33.8	CPD-59 2698	B2 V		3.57	2.6	2.34e-7	29.64	−7.51
10 47 14.42	−60 06 01.1	HD 93632B	B2 Vn		3.88	2.3	1.82e-7	29.54	−7.93
10 47 19.19	−59 27 33.5	HD 303402	B1 V		4.22	5.7	5.72e-7	30.03	−7.77
10 47 22.09	−60 05 57.6	LS 1914	B0.5 Vn		4.00	2.1	1.58e-7	29.48	−8.11
10 47 44.32	−59 52 30.9	HD 93695	B3 V		4.80	7.8	3.54e-7	29.82	−8.56
10 49 08.96	−59 53 27.7	HD 305602	B2 V		4.02	4.1	1.85e-7	29.54	−8.06
10 49 13.64	−60 11 03.2	HD 93911	B2.5 Iab		4.72	2.6	2.17e-7	29.61	−8.69

Note. The X-ray luminosities have been corrected for the interstellar absorption only (see the text).

obvious that the X-ray luminosity is thus not a constant for the majority of B stars. The B stars described in the above sections simply correspond to the tip of the iceberg, i.e., the X-ray-brightest cases. This range in X-ray luminosity implies a variety of emission processes in B stars; stellar winds and magnetic fields of various strengths, as well as different PMS companions in various states of flaring, could explain this variety of behaviors.

Note that the same conversion factors were used to derive upper limits for the 71 undetected sources. Table 6 provides the position and the stellar identification of the source (Columns 1–3), the spectral type (Column 4), the binary status (Column 5), the bolometric luminosity (Column 6), the upper limit on the number of net counts in the 0.5–8.0 keV band (Column 7), the upper limit on the associated photon flux (Column 8), the upper limit on the absorption-corrected X-ray luminosity (Column 9), and the upper limit on the L_X–L_{BOL} ratio in the total energy band (Column 10). These upper limits correspond to the upper limit of the 68% confidence interval, i.e., they are $\sim 1\sigma$ upper limits. It is interesting to note, however, that the upper limit on the L_X–L_{BOL} ratio is quite low for the two undetected O-type stars, being at least 1 dex below the average value. Without better knowledge of these two stars, this surprising result remains unexplained. The case of the undetected B stars is discussed in more detail in Evans et al. (2011).

8. SUMMARY AND CONCLUSION

The CCCP has detected the X-ray emission of 129 OB stars in the Carina Nebula (or about 65% of the massive stars present in the field of view). Among these, 78 sources display enough counts to be analyzed spectroscopically, at least roughly, and our *Chandra* observations therefore triple the number of massive stars studied in the Carina Nebula.

L_X–L_{BOL} ratios (where X-ray luminosities are corrected for ISM absorption) were estimated for a large number of different cases. For single O-type stars, $\log(L_X/L_{BOL})$ is found to be -7.26 with a very small dispersion (0.2 dex). There are only three clearly X-ray-overluminous objects: the binary HD 93403 and the putative single stars HD 93250 (a binary candidate) and Tr16 MJ 496 (a magnetic candidate?). No significant differences (at the 1% level) in the ratio values are found when comparing single stars and binaries (although the ratios are systematically slightly larger for binaries, whatever the energy band considered), bright and faint stars, early and late stars, or main-sequence stars, giants, and supergiants. A trend of harder X-ray emission for the brighter stars is detected, but with a lot of scatter. Weak-wind stars appear to emit similar amounts of X-rays compared to "normal" O stars, but their X-ray emission may be slightly softer in character.

For the few X-ray-bright B stars (i.e., those with >50 counts), the X-ray luminosity appears rather constant in the total and medium energy bands, and the spectra are harder than for O stars. When looking simultaneously at O and B stars, it seems that there is a soft transition from the latest-O to the X-ray bright, earliest-B stars. This may suggest that, for these few X-ray bright B-stars, an emission mechanism declines toward lower luminosities (the wind-shock model) while another one takes the lead (magnetic confinement?).

The authors thank J. McArthur for providing 0th order spectra of some of the piled-up sources, enabling comparison with the reconstructed data. The authors also thank the anonymous referee for his/her help. Y.N. also thanks her daughter Anaïs Céleste for letting her finish this paper while she was only one week old. Y.N. acknowledges support from the Fonds National de la Recherche Scientifique (Belgium), the PRODEX XMM and Integral contracts, and the "Action de Recherche Concertée" (CFWB-Académie Wallonie Europe). L.O. acknowledges DLR grant 50 OR 0804 (LMO), J.M.P. thanks the Royal Society for funding a University Research Fellowship, and D.C. acknowledges support from the *Chandra* grant G09-0019B. The Space Telescope Science Institute is operated by AURA, Inc., under NASA contract NAS5-26555. This work is supported by *Chandra X-ray Observatory* grant GO8-9131X (PI: L. Townsley) and by the ACIS Instrument Team contract SV4-74018 (PI: G. Garmire), issued by the *Chandra* X-ray Center, which is operated by the Smithsonian Astrophysical Observatory for and on behalf of NASA under contract NAS8-03060.

Facility: CXO (ACIS)

Note added in proof. In October 2010, just before this paper was submitted, the *Chandra* X-ray Center announced the discovery of a hook-shaped feature in the *Chandra* PSF[16], extending $\sim 0.8''$ from the main peak and containing $\sim 5\%$ of the flux. The validity of up to 18 of the $>14{,}000$ CCCP point sources ($\sim 0.1\%$) may be called into question due to this PSF feature. Those sources are flagged in the "CCCP X-ray Sources and Properties" table in Broos et al. (2011).

REFERENCES

Albacete Colombo, J. F., Flaccomio, E., Micela, G., Sciortino, S., & Damiani, F. 2007, A&A, 464, 211
Antokhin, I. I., Rauw, G., Vreux, J.-M., van der Hucht, K. A., & Brown, J. C. 2008, A&A, 477, 593
Berghöfer, T. W., Schmitt, J. H. M. M., Danner, R., & Cassinelli, J. P. 1997, A&A, 322, 167
Broos, P. S., Townsley, L. K., Feigelson, E. D., Getman, K. V., Bauer, F. E., & Garmire, G. P. 2010, ApJ, 714, 1582
Broos, P. S., et al. 2011, ApJS, 194, 2 (CCCP Catalog Paper)
Carraro, G., Romaniello, M., Ventura, P., & Patat, F. 2004, A&A, 418, 525
Cassinelli, J. P., & Olson, G. L. 1979, ApJ, 229, 304
Chlebowski, T. 1989, ApJ, 342, 1091
Cohen, D. H., Cassinelli, J. P., & Macfarlane, J. J. 1997, ApJ, 487, 867
Combi, J. A., et al. 2011, BSRSL, 80, 644
Cudworth, K. M., Martin, S. C., & Degioia-Eastwood, K. 1993, AJ, 105, 1822
DeGioia-Eastwood, K., Throop, H., Walker, G., & Cudworth, K. M. 2001, ApJ, 549, 578
Evans, N. R., Schlegel, E. M., Waldron, W. L., Seward, F. D., Krauss, M. I., Nichols, J., & Wolk, S. J. 2004, ApJ, 612, 1065
Evans, N. R., et al. 2011, ApJS, 194, 13 (CCCP Tr16 B Stars Paper)
Gagné, M., Oksala, M. E., Cohen, D. H., Tonnesen, S. K., ud-Doula, A., Owocki, S. P., Townsend, R. H. D., & MacFarlane, J. J. 2005, ApJ, 628, 986
Gagné, M., et al. 2011, ApJS, 194, 5 (CCCP Massive Star Signatures Paper)
Getman, K. V., Feigelson, E. D., Grosso, N., McCaughrean, M. J., Micela, G., Broos, P., Garmire, G., & Townsley, L. 2005, ApJS, 160, 353
Grillo, F., Sciortino, S., Micela, G., Vaiana, G. S., & Harnden, F. R., Jr. 1992, ApJS, 81, 795
Güdel, M., & Nazé, Y. 2009, A&AR, 17, 309
Güdel, M., et al. 2007, A&A, 468, 353
Harnden, F. R., Jr., et al. 1979, ApJ, 234, L51
Howarth, I. D., Siebert, K. W., Hussain, G. A. J., & Prinja, R. K. 1997, MNRAS, 284, 265
Lindgren, B. W. 1968, Statistical Theory (3rd ed.; New York: Macmillan)
Marcolino, W. L. F., Bouret, J.-C., Martins, F., Hillier, D. J., Lanz, T., & Escolano, C. 2009, A&A, 498, 837
Martins, F., Schaerer, D., & Hillier, D. J. 2005, A&A, 436, 1049
Martins, F., Schaerer, D., Hillier, D. J., Meynadier, F., Heydari-Malayeri, M., & Walborn, N. R. 2005, A&A, 441, 735
Nazé, Y. 2009, A&A, 506, 1055
Nazé, Y. 2011, BSRSL, 80, 109
Nazé, Y., Rauw, G., & Manfroid, J. 2008, A&A, 483, 171

[16] http://cxc.harvard.edu/ciao/caveats/psf_artifact.html

Nelan, E. P., Walborn, N. R., Wallace, D. J., Moffat, A. F. J., Makidon, R. B., Gies, D. R., & Panagia, N. 2004, AJ, 128, 323
Oskinova, L. M. 2005, MNRAS, 361, 679
Owocki, S. P., & Cohen, D. H. 1999, ApJ, 520, 833
Pallavicini, R., Golub, L., Rosner, R., Vaiana, G. S., Ayres, T., & Linsky, J. L. 1981, ApJ, 248, 279
Parkin, E. R., et al. 2011, ApJS, 194, 8 (CCCP QZ Car Paper)
Pittard, J. M., & Parkin, E. R. 2010, MNRAS, 463, 1657
Povich, M. S., et al. 2011, ApJS, 194, 6 (CCCP Massive Star Candidates Paper)
Rauw, G., Nazé, Y., Fernández Lajús, E., Lanotte, A. A., Solivella, G. R., Sana, H., & Gosset, E. 2009, MNRAS, 398, 1582
Rauw, G., Vreux, J.-M., Stevens, I. R., Gosset, E., Sana, H., Jamar, C., & Mason, K. O. 2002, A&A, 388, 552
Sana, H., Rauw, G., Nazé, Y., Gosset, E., & Vreux, J.-M. 2006, MNRAS, 372, 661
Sanz-Forcada, J., Franciosini, E., & Pallavicini, R. 2004, A&A, 421, 715
Seward, F. D., Forman, W. R., Giacconi, R., Griffiths, R. E., Harnden, F. R., Jr., Jones, C., & Pye, J. P. 1979, ApJ, 234, L55
Skiff, B. A. 2009, Catalogue of Stellar Spectral Classifications, VizieR Catalog B/mk/mktypes (Lowell Observatory), 1, 2023
Smith, R. K., Brickhouse, N. S., Lieadhl, D. A., & Raymond, J. C. 2001, ApJ, 556, L91
Stelzer, B., Flaccomio, E., Montmerle, T., Micela, G., Sciortino, S., Favata, F., Preibisch, T., & Feigelson, E. D. 2005, ApJS, 160, 557
Townsley, L. K., Feigelson, E. D., Montmerle, T., Broos, P. S., Chu, Y.-H., & Garmire, G. P. 2003, ApJ, 593, 874
Townsley, L. K., et al. 2011, ApJS, 194, 1 (CCCP Intro Paper)
ud-Doula, A., & Owocki, S. P. 2002, ApJ, 576, 413
ud-Doula, A., Townsend, R. H. D., & Owocki, S. P. 2006, ApJ, 640, L191
Vink, J. S., de Koter, A., & Lamers, H. J. G. L. M. 2000, A&A, 362, 295
Vuong, M. H., Montmerle, T., Grosso, N., Feigelson, E. D., Verstraete, L., & Ozawa, H. 2003, A&A, 408, 581
Walborn, N. R. 1995, RevMexAA Conf. Ser., 2, 51
Walborn, N. R. 2009, in STScI Symp. Ser. 20, Massive Stars from Pop. III and GRBS to the Milky Way, ed. M. Livio & E. Villaver (Cambridge: Cambridge Univ. Press), 167
Walborn, N. R., Nichols, J. S., & Waldron, W. L. 2009, ApJ, 703, 633
Wang, J., Townsley, L. K., Feigelson, E. D., Broos, P. S., Getman, K. V., Román-Zúñiga, C. G., & Lada, E. 2008, ApJ, 675, 464
Wilms, J., Allen, A., & Mc Cray, R. 2000, ApJ, 542, 914